BILINGUAL PUBLISHING CO.
Pioneer of Global Academics Since 1984

Organic Polymer Material Research

Volume 4 | Issue 1 | June 2022 | ISSN 2661-3875（Online）

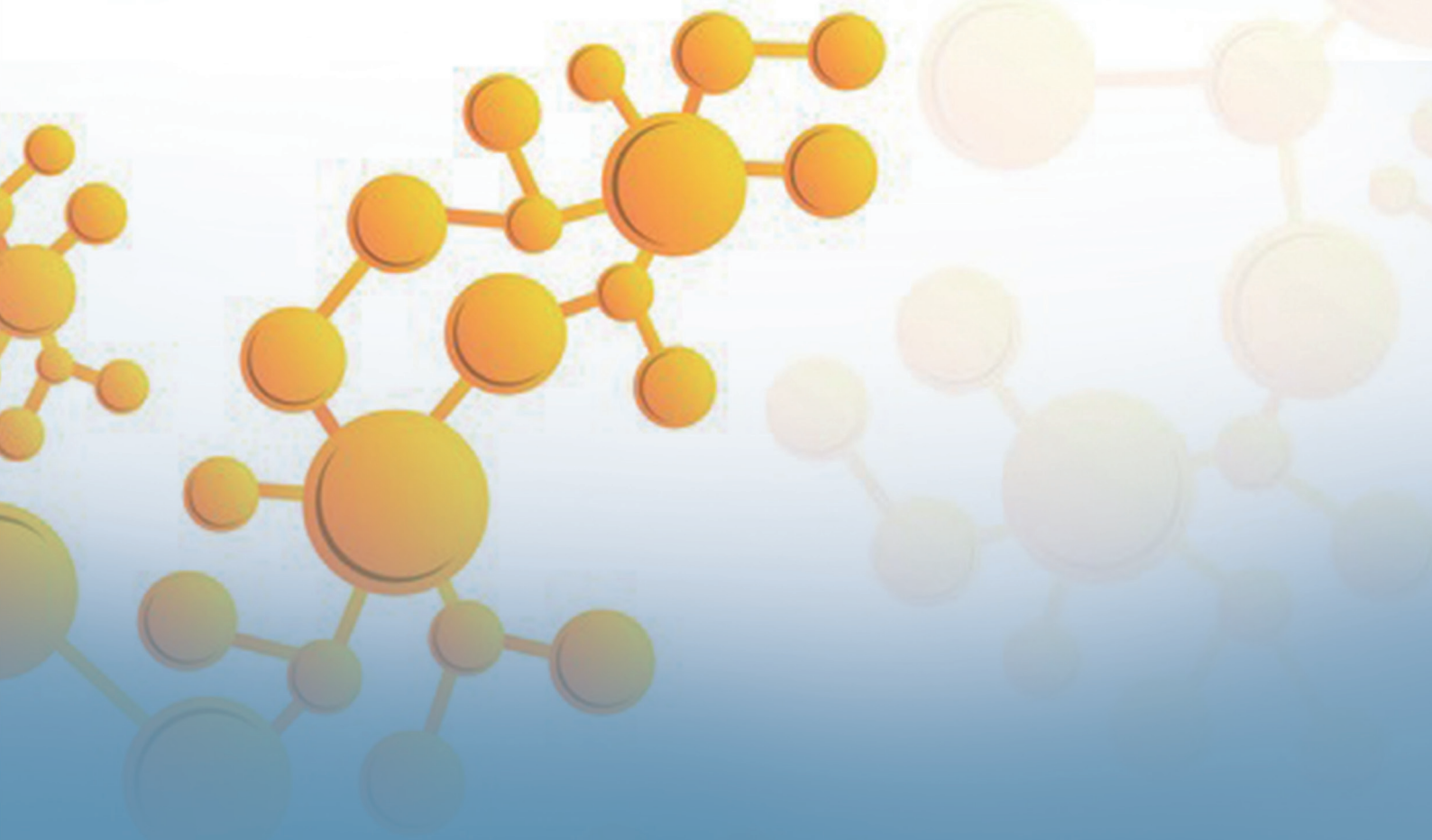

Volume 4 Issue 1 • June 2022 • ISSN 2661-3875 (Online)

Organic Polymer Material Research

BILINGUAL PUBLISHING CO.
Pioneer of Global Academics Since 1984

BILINGUAL PUBLISHING CO.
Pioneer of Global Academics Since 1984

Volume 4 | Issue 1 | June 2022 | Page1-43
Organic Polymer Material Research

Contents

Articles

Reviews

BILINGUAL PUBLISHING CO.
Pioneer of Global Academics Since 1984

Organic Polymer Material Research
https://ojs.bilpublishing.com/index.php/opmr

REVIEW

A Brief Review on Fundamentals of Conductive Polymer (CPs)

Subhadeep Chakraborty Rahul Chatterjee Abhijit Bandyopadhyay*

Department of Polymer Science and Technology, University of Calcutta, 92, A.P.C. Road, Calcutta, 700009, India

ARTICLE INFO

Article history
Received: January 23, 2022
Accepted: February 28, 2022
Published Online: 9 March 2022

Keywords:
Polymers
Conducting
Synthesis
Optical properties
Structures

ABSTRACT

Polymers are huge compounds made up of numerous monomers (repeated subunits). They have similar macro and micro properties, as well as electrical transport qualities, semiconductive capabilities, and optical features. With the advent of conductive polyacetylene, conductive polymers have gotten a lot of interest. These conductors have a wide range of electrical conductivity, which may be produced by doping, while being mechanically flexible and having a high thermal stability. Polymers may be created using a variety of methods, including chemical and electrochemical polymerization. With advancement in material stability and greater property control, an increasing variety of new applications are now being investigated.

1. Introduction

A polymer is a natural as well as manmade substance consisting of large molecules called macromolecules that are multiples of minor chemical units known as monomers. Polymer is derived from the Greek words Poly, means many, and Mers, means parts [1].

Conducting polymers or more precisely, intrinsically conducting polymers (ICPs) are organic polymers are that conduct electricity as a result of delocalization of electrons. The polymer becomes good conductors of electricity only when one electron is withdrawn from the valence band by oxidation process, called p-doping or introduced to the conducting band by reduction, called n-doping. The concentration of charge carriers i.e. number of charges per unit volume and their mobility μ, or how quickly they can travel in the material, determine a material's conductivity. Temperature has a significant impact on conductivity. Conductivity reduces with rising temperature of metals, but that increases for semi-conductors. Fine tuning of the electrical characteristics is achieved by modified organic synthesis and sophisticated dispersion methodology [1].

Conducting polymers have a wide range of applications in the field of variety of innovative technical gadgets, in-

**Corresponding Author:*
Abhijit Bandyopadhyay,
Department of Polymer Science and Technology, University of Calcutta, 92, A.P.C. Road, Calcutta, 700009, India;
Email: abpoly@caluniv.ac.in

DOI: https://doi.org/10.30564/opmr.v4i1.4395

cluding electrochromic displays, photovoltaic devices, and biosensors. Conducting polymers or organic metals may one day replace traditional inorganic metal in a number of key applications [2]. Certain features of inorganic metals, such as their lack of environmental friendliness and high toxicity, that's why these organic metals could be useful as alternatives. Conducting polymers have light emitting properties, for this reason it can be used in LEDs, Diodes, Photovoltaic cells etc. In our previous studies, Sardar et al. said the light emitting behavior of perovskite was tuned and also the water degradability studies reveal that conducting polymers enhanced the life time of perovskite [3].

Conducting polymers shows high optical and electrical properties when it is irradiated with visible light having high photon adsorption co-efficiency. Thus, it can be used in the degradation of soluble toxic materials present in water [4,5]. Midya et al. had synthesized by in-situ carbon dot (CDs) deposited functionalized chitosan (polypyrrole grafted chitosan) with increased photocatalytic activity towards degradation of hazardous 2-chloro phenol (2-CP) into tiny molecules [6].

2. History of Conducting Polymers

Conductive polymers are a sub-gathering of a bigger, more established gathering of natural and inorganic electrical conductor. Indeed, as soon as 1862 H. Letheby of the College of London Hospital, by anodic oxidation of aniline in Sulfuric corrosive, got a somewhat conductive material which was likely polyaniline [7]. In the mid 1970s, it was tracked down that the inorganic explosion polymer, poly(sulphur nitride) $(SN)_x$, was superconductive at amazingly low temperatures (T_c=0.26 K).

Polyacetylene (PA)

Polyacetylene (PA) was unintentionally manufactured by Shirakawa in the 70's. It is the very first polymer prepared to do directing electricity. It is a natural polymer with the rehashing unit $(C_2H_2)_n$. The creation of exceptionally directing PA prompted the fast mission in research for the disclosure of new conductive polymers [8-10].

Poly (thiophene)

Another Poly (thiophene) subsidiary was created by two researchers at the Bayer AG research labs in Germany in 1980. Poly (thiophene) (PTh) that makes the naturally and thermallystable materials utilized as electrical super capacitor, non-straight optics, PLEDs, eletrochromics, photo resists, solar cell, antistatic coatings etc. [11-15].

Polypyrrole (PPy)

Polypyrrole (PPy) is a sort of natural polymer shaped by pyrrole polymerization. It was demonstrated to be a conductive polymer in 1968. Among the various leading polymers, PPy has been generally examined, because of its simplicity of readiness, unrivaled redox properties balanced out oxidized structure, ability to give transcending conductivity, water dissolvability, industrially available and important electrical and optical properties.In 1963 Weiss and collaborators clarified the pyrolysis of tetraiodopyrrole to manufacture shockingly conductive materials. In 1979, a superior electrochemical procedure was utilized to incorporate detached movies with sufficiently great mechanical properties to concentrate on this framework as a conductive polymer [16-20].

PEDOT

Poly (3,4ethylenedioxythiophene) (PEDOT) is a directing polymer in view of 3,4 - ethylene dioxylthiophene monomer. PEDOT enjoys a few benefits which remembers optical straightforwardness for meager, oxidized movies, high strength, sensible band hole and low redox potential. It has used in many fields like transparent electrodes for thick-film electroluminescence, source gate and drain in the quickly developing organic semi-conductors [21-24].

Poly (phenylene vinylene) (PPV)

Poly (phenylene vinylene) (PPV) is a diamagnetic substance, equipped for electroluminescence and has amazingly low electrical conductivity. PPV is exceptionally glasslike, precisely solid and naturally steady. The conductivity is improved by doping with iodine, ferric chloride, soluble base metals or acids however with less steadiness [25,26-30].

Polyphenylene and Polyparaphenylene (PPP)

Polyphenylene and Polyparaphenylene (PPP) are predecessors to a rigid-rod polymeric host family conductive polymer made up of repeating p-phenylene units that is transformed to its conducting state using an oxidant or a dopant. PPP was doped in 1980 to achieve conductivity equivalent to PA. It's the first time a nonacetylenic hydrocarbon polymer has been doped with either an electron donor or an electron acceptor to provide conducting characteristics [31-34].

The chemical structures of the mentioned conductive polymers were illustrated in Figure 1.

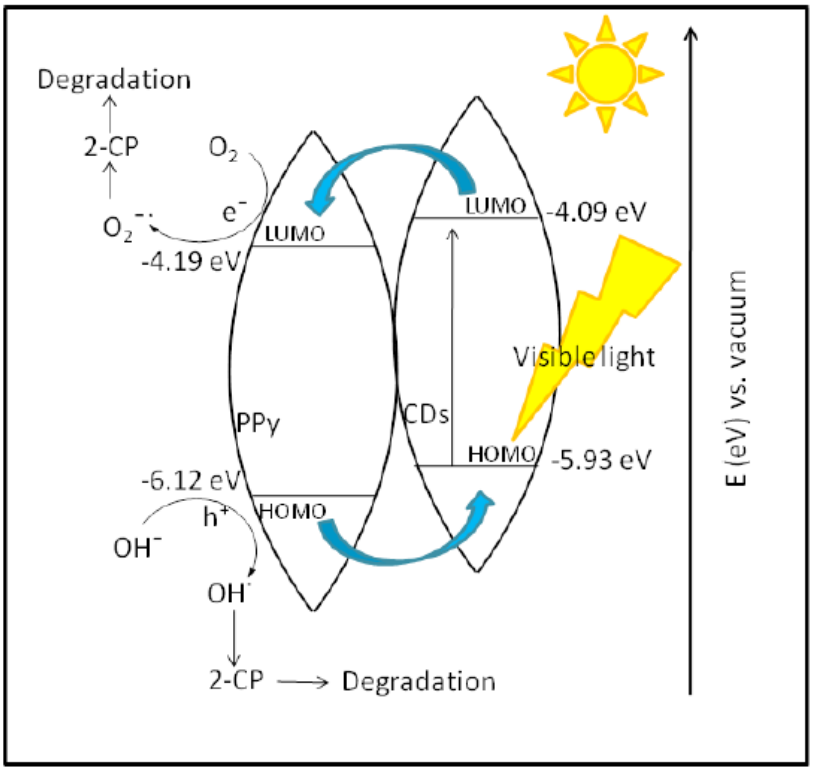

Figure 1. Proposed photocatalytic degradation mechanism of 2-CP using Ch-g-PPy@CDs under sunlight exposure, Reprinted with permission from ref. [6]

3. The structures of Conducting Polymers

Conductors or metals, insulators, and semiconductors are the three primary categories of materials. They are distinguished by their capacity to conduct current or allow current to flow through them. The structures of various conducting polymers have been shown in Figure 2. Although certain strongly conducting polymers, such as polyacetylene, fall into the metal range, conducting polymers are often categorised as semiconductors. The physical characteristics of conducting polymers as follows in Table 1 [2].

Table 1. Properties of conducting polymers

Property	Conducting polymers
Electrical conductivity(S/cm)	10^{-11} - 10^{3}
Carriers	Electrons of conjugated double bonds
Concentration of carriers per cm^3	10^{12} - 10^{19}
Effect of impurity	Impurities of 0.1% - 1% change conductivity by 2 to 3 orders of magnitude
Magnetic properties	Paramagnets

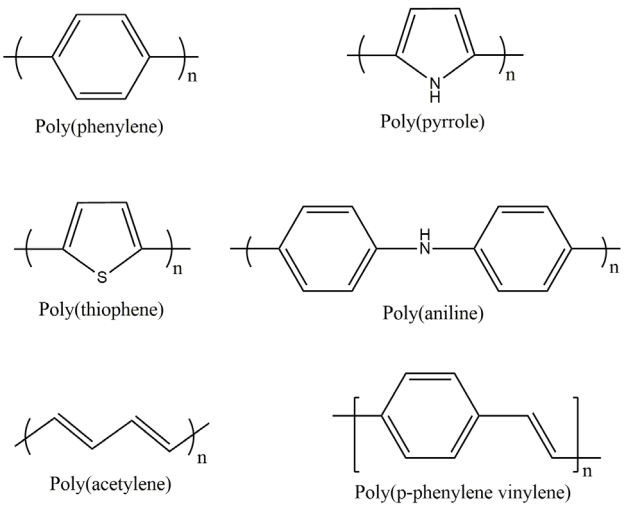

Figure 2. Chemical structures of conducting polymers

4. What is Electrical Conductivity?

Conductivity defined by the Ohm's law that is,

$$V = IR$$

Where R is the resistance, I is the current and V is the voltage present on the material. The conductivity depends on number of charge of the material and their mobility.

There are three types of conduction.

i) Intrinsic conductivity: conduct electricity in pure form by present of electrons and holes.

ii) Extrinsic conductivity: by adding external impurities called as doping. Several doping methods have used to make conjugated double bonds, like redox doping, non redox doping, photo doping, charge injection doping.

iii) Holes: created by removal of electrons on doping [35].

Conducting mechanism

While "doping" refers to the addition of a donor or acceptor molecules to a polymer, the reaction that occurs is really a redox reaction.

The production of a soliton or polaron, which is a cation (or anion) radical, is the first stage.

$Pn \Leftrightarrow [Pn^{+} A^{-}]$

This phase may be referred to as the second electron transfer, resulting in the production of a bipolaron dication (or dianion).

$[Pn^{+} A^{-}] \Leftrightarrow [Pn^{2+} 2A^{-}]$

When feasible, charge transfer compounds may develop between energized and neutral portions of the polymer following the initial redox event.

$[Pn\bullet^{+} A^{-}] + Pm \rightarrow [(Pn\ Pm)\bullet^{+} A^{-}]$

5. Synthesis of Conducting Polymers

1) Chemical synthesis: Conducting polymers are created chemically by oxidising or reducing monomers and polymerizing the matching monomers. The main benefit is the possibility of mass manufacturing at a reasonable cost. Several studies have been conducted to improve the quality and quantity of manufactured products produced using the oxidative polymerization process. The employment of electrochemical techniques is not mandated by the principles of chemical methods. Poly (3-hexylthiophene), for example, is the most researched conducting polymer that is virtually always made chemically. Chemically, PPy and PANI may be synthesized. After conjugation, the most important need for chemical polymerization is stability. Oligomers and low molecular weight polymers must be reactive and soluble enough to polymerize for chemical polymerization to be successful. If an oligomer precipitates out of solution, polymerization should proceed in a heterogeneous manner, which is becoming increasingly implausible as monomer and reactive polymer concentrations decrease.

2) Electrochemical synthesis: Conducting polymers are made electrochemically by either anodic oxidation or cathodic reduction of suitable electroactive functional monomers. Because of its simplicity, cost-effectiveness, and ability to accomplish the process in a single section glass cell, electrochemical synthesis of conducting polymers is a very essential approach. Typically, the potential for monomer oxidation to lead to polymerization is greater than the potential for oligomeric intermediate polymerization. Alternate chemical and electrode reaction stages are used in a simplified method of electro polymerization of an electro active monomer, such as pyrrole or thiophene.

3) Photochemical method: Photochemical preparation has been claimed to have a number of advantages as a consequence of its rapid and low-cost process, as well as the fact that it is not harmful to the environment. The process can be used to create certain conductive polymers. Pyrole, for example, has been successfully polymerized to Poly pyrrole by irradiation with visible light, either as the photosensitizer or as an electron acceptor. Currently, horseradish peroxide is used to begin aniline polymerizations in the presence of hydrogen peroxide via oxidative free radical coupling reactions. When compared to chemical and electrochemical approaches, aniline polymerization may be accomplished under more benign conditions.

4) Metathesis method: Metathesis is a chemical process in which one portion of each substance is swapped, resulting in the formation of two new compounds. Ring-opening metathesis of cyclo-olefins, acyclic or cyclic metathesis of alkynes, and diolefin metathesis are the three types of metathesis polymerization.

5) Concentrated emulsion method: The emulsion technique of polymerization is a heterophase approach with three segments: water, latex particle, and monomer droplet. A radical polymerization is the main process at work. Bulk and solution polymerization have one segment in the arrangement, with the monomer as the solvent and the initiator in the same segment. Until significantly changed, the produced polymer remains soluble in either the monomer or the solvent. A micelle-forming surfactant, a water-soluble initiator, and a water insoluble monomer are all used in this method.

6) Inclusion method: At the atomic or molecular level, inclusion polymerization creates composite materials. This sort of polymerization can pave the way for one-of-a-kind low-dimensional composite materials with huge promise. An electroconductive polymer, for example, may be used to make a molecular wire. On this point, organic hosts have been used to create composites of such polymers. This polymerization, according to Miyata et al., may be regarded as a common space-dependent polymerization and should not be viewed just through the lens of stereoregular polymerization.

7) Solid state method: Solid State polymerization is a process in which the lengths of polymer chains are lengthened by heat in the absence of oxygen and water, either by vacuum or by removing by-products with an inert gas. Temperature, pressure, and the diffusion of by-products

from the pellet's core to the shell govern the reaction. It's frequently used after melt polymerization to improve polymer mechanical and rheological characteristics before injection blow moulding. The solid state approach is widely used in the manufacturing of bottle-grade PET, films, and sophisticated industrial fibres in industry. The use of simple and inexpensive apparatus, as well as the avoidance of some of the issues associated with traditional polymerization techniques, are the main advantages of solid-state polymerization.

8) Plasma polymerization: Plasma polymerization is an unique method for producing thin films from a variety of organic and organometallic precursors. Plasma polymerized films are insoluble, thermally durable, chemically inert, and mechanically robust because they are pinhole-free and strongly cross linked. Such films are also exceedingly coherent and sticky to a variety of substrates, including traditional polymer, glass, and metal surfaces. They have been widely employed in recent years for a variety of applications, including perm selective membranes, protective shells, biological materials, electrical, optical devices, and adhesion supports, due to their exceptional qualities [36-38].

9) Vapour phase polymerization: Vapour phase polymerization (VPP) is a well-known method for introducing a monomer in vapour form to an oxidant-coated substrate. At the oxidant vapour contact, polymerization occurs. VPP is a method for immobilizing materials on a modified electrode surface [39,40].

6. Characterization

Conducting polymers, like many other polymers, may be described using a number of analytical methods. There are several examples in the literature, including:

a) Cyclic voltammetry - in order to better understand redox processes in conjugated polymers and to assess prospective cell and electrochromic window component choices. Murugappan et al. had synthesized a conducting polymer poly (3,4-ethylenedioxythiophene) (PEDOT) by electrochemical procedure and characterized by cyclic voltammetry method. The decrease of the polymer generated on the surface as a result of process I causes the peak at roughly 0.8 V. A new peak occurs at roughly +0.4 V on the second CV scan (red trace). This peak is caused by polymer oxidation, which did not occur until after polymer synthesis during the initial CV scan (black) [41]. Li et al. in one of their studies revealed the synthesis of three 3,4-bis(alkylthio)pyrroles by a nonclassical pyrrole ring formation reaction followed by alkylation of the dithiol-2-one functional group. The synthesized polymers were investigated by cyclic voltammetry study. The CV study shows that the monomers have much less oxidation potentials than that of virgin pyrrole [42].

b) Nuclear magnetic resonance - for determining the structure of the insoluble organic conducting polymers, solid state NMR spectroscopy can be employed. Zujovic et al. had studied the molecular dynamics in complex and diverse material using solid state NMR (SSNMR) technology for polyaniline (PANI) SSNMR can offer crucial information on the structure and conformation of the polymer backbone, as well as the type and distribution of charge carriers, when applied to PANI [43]. Wahane et al. studied the structure of poly pyrrole by using various spectroscopic analysis techniques. High resolution NMR Spectroscopic methods have emerged into the most powerful tool for studying the structure of such conducting polymers in solution and in solid form. Chemical oxidation polymerization in non-aqueous media was used to make several PPy / Metal Oxide composites, which were then analysed by NMR [44].

c) Raman analysis - Hiragond et al. synthesized polythiophene (PTh), polypyrrole (PPy) and polyaniline (PANI) by oxidative coupling method. CdS/polythiophene (CdS/PTh), CdS/polypyrrole (CdS/PPy) and CdS/polyaniline (CdS/PANI) hybrid nanocomposites had been synthesized. The interaction of CdS with these conjugated polymers in the current hybrid nanocomposites was further validated by Raman spectroscopy of all samples. Raman spectra of CdS/PTh, CdS/PPy, and CdS/PANI nanocomposites in the range of 100-1800 cm^{-1}. Various peaks of vibrational Raman active modes were identified in all samples, with two peaks in the area of 300-400 cm^{-1} matching to fundamental optical phonon modes (LO and 1LO+E2) of CdS QDs [45]. Xu et al. synthesized PANI/$Bi_{12}O_{17}Cl_2$ composites at room temperature via a green and simple approach. The as-prepared PANI/$Bi_{12}O_{17}Cl_2$ composite was also tested using Raman spectroscopic technology. The distinctive bands at 149 cm^{-1} and 94 cm^{-1} in the Raman spectra of $Bi_{12}O_{17}Cl_2$ corresponded to the A1g internal Bi-Cl and Eg internal Bi-Cl stretching modes, respectively [46].

d) Electroluminescence - to see if it might be used in light-emitting diodes (LEDs). Krishnaswamy et al. had deposited high quality P-type Polypyrrole (PPy) on ITO by Pulse Laser deposition (PLD) technique. Optical characteristics were investigated in depth. The thin film had a transmittance of 59.7% and a reduced band gap of 1.73 eV. The PPy thin sheet has an optical conductivity of 0.27 S/cm. The dielectric characteristics of the PPy thin film were thoroughly examined. The photoluminescence spectra of a PPy thin film at room temperature showed three peaks at 373 nm, 425 nm, and 486 nm, corresponding to electronic transitions, polarons, and bipolarons, respectively. PPy thin films with high luminescence efficiencies can be

employed as an excellent hole transport layer [HTL] in electroluminescence devices [47].

(e) X-ray analysis, including Rutherford backscattering - to acquire insight into the conducting process by understanding the crystal structure and obtaining elemental thickness profiles [2]. Sardar et al. studied the synthesis of a smart composite from poly (3-bromothiophene) (PTBr) and graphene quantum dot (GQD) through facile in-situ and ex-situ routes. The crystallographic structure of the composites were analyzed by XRD. The diffraction pattern of neat poly (3-bromothiophene) (PTBr) was broad, indicating that it was mostly amorphous (low percentage crystallinity of 26 percent). It had a reflection peak at 2-26 degrees, which corresponded to the reflection from the (002) plane. The reflection angle in the in-situ composite was lowered to 24.8 °, whereas it was further reduced to 23.4 ° in the ex-situ sample [3].

7. Applications of Conductive Polymers(CP)

Drug delivery

Current drug-delivery technologies are effective in delivering pharmaceuticals in a regulated manner. and it is depicted in Figure 3. The application, however, is still limited to cell clusters instead of individual cells. Developing innovative medicine delivery methods will open up new possibilities that were previously unavailable due to the limitations of existing oral formulations. The use of conductive polymers in bioanalytical sciences is gaining a lot of attention because of their biocompatibility, which allows them to be used in in vivo biosensor applications for constant monitoring of medications or metabolites in bodily fluids.

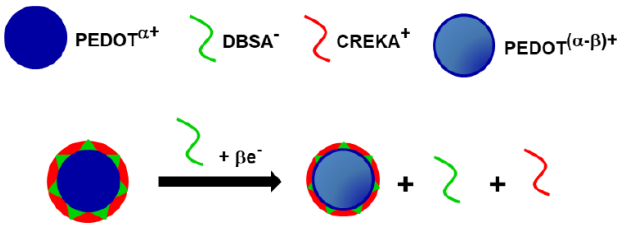

Figure 3. The mechanism of peptide release from CREKA/PEDOT NPs. Reproduced with permission from ref. [48]

Tissue engineering

The medical sectorsis one of the sectors that might be transformed by the uses of conductive polymers, particularly in tissue engineering and biosensors. Electrospinning allows for the creation of 3D scaffolds made of conductive polymers. Because conductive polymers are a good biocompatible matrix for biomolecules, they're of particular interest.PEDOT, on the other hand, has lately attracted a lot of attention due to its improved electrical conductivity and chemical stability. Now a days PEDOT uses by growing neural cells in an in vitro dorsal root ganglion model, in film and nanotube morphology.

Bioactuators

Bioactuators are mechanical force-generating gadgets that may be utilised to construct artificial muscles. Bioactuators have been built using the phenomena of change in the volume of the CP scaffold when electrical stimulation is applied. Two layers of CP are used in a triple layer configuration in artificial muscle operations, with the intermediate layer consisting of a non-conductive substance.

Smart textiles

Fabrics that can sense exterior situations or stimuli such as chemical, thermal, electrical, photonic, magnetic, and the like are known as smart textiles. It can intelligently respond to and adapt to external behaviour. Conductive polymers have been intensively studied for smart textiles in recent years. There are now around twenty five conducting polymers being investigated for such uses [39,40]. Because of their reduced weight, high control can be done, cheap cost, tunable electrical conductivity, bio compatibility, and customise ability to provide a sensing and actuating function, these polymers were chosen [49].

Self-healing conductive material

Self-healing materials are intelligent materials that can regain some or all of their properties after being injured from the outside. Self-healing properties are a potential technique to make materials more durable and dependable. Extrinsic and intrinsic self-healing mechanisms are two types of self-healing mechanisms. In extraneous self-healing instrument, mending process is relying upon the microcapsules/pipelines containing recuperating specialist and intrinsic self-recuperating component, recuperating process relies upon the powerful reversible substance bond making capacity of the framework upon the feeling of an outer boost, for example, temperature, dampness, light, electrical flow through reversible sol-gel progress. The highly conductive PEDOT: PSS is being investigated as a self-healing conductive material. Adding a little quantity of the quasi surfactant plasticizer Triton-100 ($C_{14}H_{22}O[C_2H_4O]_n$) to PEDOT (n = 9-10): PSS resulted in a high level of self-healing abilities [2].

Conducting polymer as wearable: The need for flexible and wearable next-generation electronic gadgets that can bend and stretch under mechanical deformation is increasing. Because of their large-area synthesis, cheap

cost, low toxicity, great flexibility, and customizable electronic characteristics, energy harvesting technologies have heavily invested in organic and polymeric semiconducting materials. Electrically conductive p-conjugated polymers, for example, have been studied in various thermoelectric technologies for producing stretchable, wearable, and light-weight thermoelectric devices that can harvest energy from a temperature gradient and produce electricity without polluting the environment or requiring moving parts [50]. Conducting polymers have also antifouling property and the mechanism which it follows is shown in Figure 4.

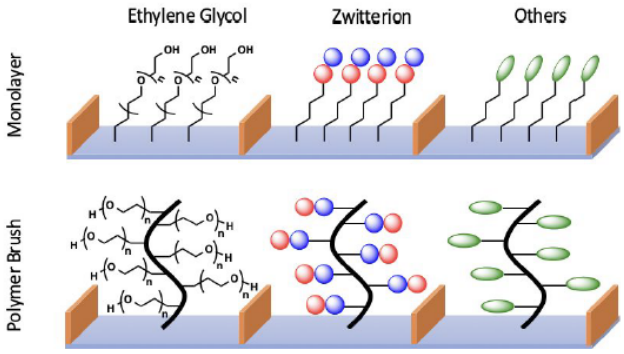

Figure 4. Design and classification of conducting polymers with an antifouling property. Reproduced with permission from ref. [51]

Supercapacitors and electrolytic-type capacitors are two further possible uses for conductive polymers. As a consequence of their multiple protonation and oxidation forms, several conductive polymers, including polyaniline, exhibit a wide range of color. Their electrochromic capabilities can be exploited to make "smart windows" that absorb solar energy in the summer. Polymers have the benefit of being produced in big sheets with limitless visual angles, as opposed to liquid crystals [52-55].

Kraft et al. (2019) [56] had synthesized PEDOT: PSS conducting polymer which has conductivity of 700 S cm^{-1}. The use of printable elastic conductors in large-area fabrication of wearable electronics and prosthetics opens up new possibilities. Furthermore, by placing sensor arrays close to the skin, they have the potential to advance health monitoring and continuous diagnostics. These devices must be comfortable to wear and must be able to withstand strains and deformations like twisting and stretching. The introduction of a conductive polymer ink for elastic interconnects and electrodes. Inkjet printing's processability allows for versatile, contactless, and maskless large-area processing. The printed PEDOT:PSS-based interconnects have conductivities of up to 700 S cm^{-1}, can withstand strains of up to 100%, and are stable in air (less than 5 percent change in resistance in 1 month). The conductivity is among the greatest recorded for inkjet-printed PEDOT:PSS, making it useful not only for stretchy circuits, but also for printed flexible and rigid PEDOT: PSS-based applications such solar cells, organic light emitting diodes, and electrochemical sensors.

Jeong et al. (2019) [57] synthesized organic and perovskite light-emitting diodes (LEDs), an ideal conducting polymer anode (CPA) requires a high electrical conductivity k, a high work function WF, and the avoidance of exciton quenching between the anode and the overlaying emitting layer. Due to their trade-off connection, boosting the k and WF at the same time has been a difficult unresolved challenge. Previous efforts to increase the WF have lowered the films' k and vice versa. To tackle this basic problem, careful molecular scale control of conducting polymer compositions is necessary. They presented a molecular scale control approach for decoupling the WF from k in a CPA while keeping exciton quenching blocking capabilities. In green polycrystalline perovskite LEDs, this adjustment resulted in a high current efficiency of 52.86 cd A-1 (10.93 percent ph el-1). Their findings offer valuable insight into the development of effective CPAs for high-efficiency organic and perovskite LEDs.

Bilal et al. (2014) [58] synthesized poly (o-toluidine) (POT), a methyl-substituted derivative of PANI, by inverse emulsion polymerization. The dispersion media was a combination of 2-butanol and chloroform, the oxidant was benzoyl peroxide, and the dopant and surfactant was dodecylbenzenesulfonic acid (DBSA). POT was collected in its salt form and found to be totally soluble in a variety of organic solvents, including DMSO, chloroform, toluene, THF, acetonitrile, and ethanol (so far the most solvents). Cyclic voltammetry, in situ UV-Vis spectroelectrochemistry, viscosity and in situ conductance measurements, FTIR, and TGA were used to characterise the produced polymer. POT has a high conductance that is comparable to electrochemically synthesised POT, according to conductance measurements. The electrochemical activity of the POT film dip-coated on a gold electrode was very stable in air; even after 14 days in the open, there was no discernible decline in the film's electrochemical activity. Thermal analysis reveals a very good thermal stability up to 513 °C. POT works as a very efficient corrosion protection layer on steel, according to potentio dynamic polarisation studies, with a 77 percent protection efficiency.

Tuken et al. (2004) [59] in a $LiClO_4$ containing acetonitrile solution, electrochemical polymerization of polythiophene (PTh) was examined on a nickel covered mild steel (MS) electrode. A 1 mm thick nickel coating was depos-

ited galvanostatically from a suitable bath solution. The PTh film was then synthesised using the cyclic voltammetry technique in 0.1 M thiophene containing ACN-$LiClO_4$. Electrochemical impedance spectroscopy (EIS) and anodic polarisation curves were used to study the corrosion performance of nickel coated samples with and without polymer top coatings in a 3.5 percent NaCl solution. MS was protected from corrosion by the nickel coating, which acted as a physical barrier. However, its barrier properties deteriorated with time, and it was unable to protect MS patients. The PTh top coat significantly increased the barrier performance, and good protection against MS corrosion was achieved over a long period of time in such a hostile environment.

Marzocchi et al. (2015) [60] synthesized poly (3,4-ethylenedioxythiophene) poly (styrene sulfonate) (PEDOT: PSS). Conducting polymers are interesting materials for tissue engineering applications because of their electrical conductivity and reversible doping, they may both offer a biocompatible scaffold for physical support of live cells and convey electrical and mechanical stimuli. Thin films of poly (3,4-ethylenedioxythiophene) poly (styrenesulfonate) (PEDOT: PSS), one of the most promising materials for bioelectronics applications, are prepared using two different techniques, spin coating and electrochemical polymerization, and their oxidation state is then changed electrochemically with the application of an external bias.

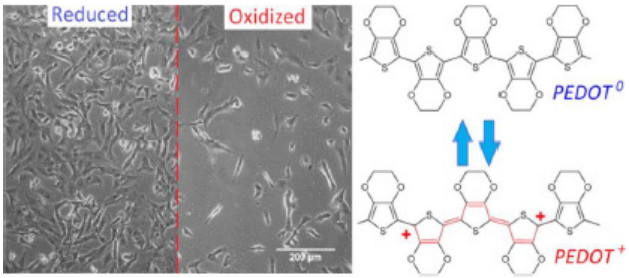

Figure 5. Structure of oxidized and reduced form of PEDOT. Reproduced with permission from ref. [60]

The electrochemical characteristics of the various kinds of PEDOT are as follows: The efficacy of the oxidation process and its stability over time are assessed using cyclic voltammetry and spectrophotometry on PSS. Their physical qualities on the surface and their relationship to PEDOT's redox state: Atomic force microscopy (AFM), water contact angle goniometry, and sheet resistance measurements are used to investigate PSS. The structure of the oxidized and reduced form of PEDOT is shown in Figure 5. Finally, primary human dermal fibroblasts (hDF) and human glioblastoma multiforme cells (T98G) are cultivated on PEDOT: PSS films with various oxidation states, revealing that the influence of the substrate on cell growth rate is substantially cell-dependent: T98G growth is aided by reduced samples, but hDF development is aided exclusively by oxidised substrates with significant chemical interactions with the cell culture medium.

8. Conclusions

In this paper we have described a variety of conductive polymers, as well as new synthetic processes that have been developed to synthesize those polymers. Among all the routes of synthesis of conducting polymers it can be concluded that chemical polymerization techniques are beneficial from the standpoint of mass manufacturing, but we must also limit by-products and waste materials in order to maintain a clean and healthy global environment. The characterization along with some vivid examples has been incorporated to have a better clarity in this regard. It has also been found that the conducting polymers have better light emitting properties. The electrical properties have been showcased by cyclic voltammetry study by scientists around the world. The wide range of applications has been included in this review. It can be said that in future these conducting materials could find its way in this smart world as we have seen that no one can think of storing for security purpose in storage device which is nothing but the contribution of these conducting materials. The LEDs have already replaced the power giant 100 W bulb and more to see in future. The smart material could also find its way into medical fields. The catalytic polymerization technique is a desirable candidate for an environmentally friendly reaction mechanism. At this moment, catalytic studies should be enhanced in order to get a more accurate conducting polymer. The authors anticipate that this study will spur more research into conductive polymers and new catalytic methods for their production.

Conflict of Interest

The authors declare no conflict of interest.

References

[1] Awuzie, C.I., 2017. Conducting Polymers. Materials Today: Proceedings. 4, 5721-5726. DOI: https://doi.org/10.1016/j.matpr.2017.06.036.

[2] Harun, M.H., Saion, E., Kassim, A., et al., 2007. Conjugated Conducting Polymers : A Brief Overview, Sensors Peterbrgh. NH. 2, 63-68. http://sedaya.edu.my/jasa/2/papers/08I.pdf.

[3] Sardar, S., Roy, I., Chakraborty, S., et al., 2021. A selective approach towards synthesis of poly (3-bromo thiophene)/graphene quantum dot composites via in-situ and ex-situ routes: Application in light emis-

sion and photocurrent generation. Electrochimica Acta. 365.
DOI: https://doi.org/10.1016/j.electacta.2020.137369.

[4] Shirzad, M., Karimi, M., 2020. Statistical analysis and optimal design of polymer inclusion membrane for water treatment by Co(II) removal. Desalination and Water Treatment. 182, 194-207.
DOI: https://doi.org/10.5004/dwt.2020.25214.

[5] Shirzad, M., Karimi, M., Abolghasemi, H., 2019. Polymer inclusion membranes with dinonylnaphthalene sulfonic acid as ion carrier for Co(II) transport from model solutions. Desalination and Water Treatment. 144, 185-200.
DOI: https://doi.org/10.5004/dwt.2019.23575.

[6] Midya, L., Chettri, A., Pal, S., 2019. Development of a Novel Nanocomposite Using Polypyrrole Grafted Chitosan-Decorated CDs with Improved Photocatalytic Activity under Solar Light Illumination. ACS Sustain. Chemical Engineering. 7, 9416-9421.
DOI: https://doi.org/10.1021/acssuschemeng.9b00615.

[7] Heeger, H., MacDiarmid, Alan J., Shirakawa, Alan G., 1974. Advanced Information - The Nobel Prize in Chemistry 2000. Nobel Media AB 2019. pp. 1-16.
DOI: https://doi.org/10.1007/978-1-84996-290-2.

[8] Zhang, C., Liu, L., Okamoto, Y., 2020. Enantioseparation using helical polyacetylene derivatives. Tractrends In Analytical Chemistry. 123, 115762.
DOI: https://doi.org/10.1016/j.trac.2019.115762.

[9] Miao, Z., Gonsales, S.A., Ehm, C., et al., 2021. Cyclic polyacetylene. Nature Chemistry. 13, 792-799.
DOI: https://doi.org/10.1038/s41557-021-00713-2.

[10] Wang, S., Sun, Q., Gröning, O., et al., 2019. On-surface synthesis and characterization of individual polyacetylene chains. Nature Chemistry. 11, 924-930.
DOI: https://doi.org/10.1038/s41557-019-0316-8.

[11] Husain, A., Ahmad, S., Mohammad, F., 2020. Synthesis, characterisation and ethanol sensing application of polythiophene/graphene nanocomposite. Materials Chemistry and Physics. 239,122324.
DOI: https://doi.org/10.1016/j.matchemphys.2019.122324.

[12] Shiraishi, Y., Matsumoto, M., Ichikawa, S., et al., 2021. Polythiophene-Doped Resorcinol-Formaldehyde Resin Photocatalysts for Solar-to-Hydrogen Peroxide Energy Conversion. Journal of the American Chemical Society. 143, 12590-12599.
DOI: https://doi.org/10.1021/jacs.1c04622.

[13] Wang, Q., Qin, Y., Li, M., et al., 2020. Molecular Engineering and Morphology Control of Polythiophene:Nonfullerene Acceptor Blends for High-Performance Solar Cells. Advanced Energy Materials. 10, 1-26.
DOI: https://doi.org/10.1002/aenm.202002572.

[14] Liang, Z., Li, M., Wang, Q., et al., 2020. Optimization Requirements of Efficient Polythiophene: Nonfullerene Organic Solar Cells. Joule. 4, 1278-1295.
DOI: https://doi.org/10.1016/j.joule.2020.04.014.

[15] Lu, Y., Wang, S., Xiong, C., et al., 2020. Synthesis and characterization of a liquid-like polythiophene and its potential applications. Synthetic Metals. 270, 116603.
DOI: https://doi.org/10.1016/j.synthmet.2020.116603.

[16] Pang, A.L., Arsad, A., Ahmadipour, M., 2021. Synthesis and factor affecting on the conductivity of polypyrrole: a short review. Polymers for Advanced Technologies. 32, 1428-1454.
DOI: https://doi.org/10.1002/pat.5201.

[17] Maruthapandi, M., Nagvenkar, A.P., Perelshtein, I., et al., 2019. Carbon-Dot Initiated Synthesis of Polypyrrole and Polypyrrole@CuO Micro/Nanoparticles with Enhanced Antibacterial Activity. ACS Applied Polymer Materials. 1, 1181-1186.
DOI: https://doi.org/10.1021/acsapm.9b00194.

[18] Sahu, S., Kar, P., Bishoyi, N., et al., 2019. Synthesis of Polypyrrole-Modified Layered Double Hydroxides for Efficient Removal of Cr(VI). Journal of Chemical & Engineering Data. 64, 4357-4368.
DOI: https://doi.org/10.1021/acs.jced.9b00444.

[19] Wang, C., Yang, M., Liu, L., et al., 2020. One-step synthesis of polypyrrole/Fe_2O_3 nanocomposite and the enhanced response of NO_2 at low temperature. Journal of Colloid and Interface Science. 560, 312-320.
DOI: https://doi.org/10.1016/j.jcis.2019.10.076.

[20] Yi, T.F., Mei, J., Peng, P.P., et al., 2019. Facile synthesis of polypyrrole-modified $Li_5Cr_7Ti_6O_{25}$ with improved rate performance as negative electrode material for Li-ion batteries. Composites Part B-Engineering. 167, 566-572.
DOI: https://doi.org/10.1016/j.compositesb.2019.03.032.

[21] Petsagkourakis, I., Kim, N., Tybrandt, K., et al., 2019. Poly(3,4-ethylenedioxythiophene): Chemical Synthesis, Transport Properties, and Thermoelectric Devices. Advanced Electronic Materials. 5, 1-20.
DOI: https://doi.org/10.1002/aelm.201800918.

[22] Jiang, Y., Liu, T., Zhou, Y., 2020. Recent Advances of Synthesis, Properties, Film Fabrication Methods, Modifications of Poly (3,4-ethylenedioxythiophene), and Applications in Solution-Processed Photovoltaics. Advanced Functional Materials. 2006213, 1-46.
DOI: https://doi.org/10.1002/adfm.202006213.

[23] Rahimzadeh, Z., Naghib, S.M., Zare, Y., et al., 2020. An overview on the synthesis and recent applications of conducting poly (3,4-ethylenedioxythiophene) (PEDOT) in industry and biomedicine. Journal of Materials Science. 55, 7575-7611.
DOI: https://doi.org/10.1007/s10853-020-04561-2.

[24] Hui, Y., Bian, C., Xia, S., et al., 2018. Synthesis and electrochemical sensing application of poly(3,4-ethylenedioxythiophene)-based materials: A review. Analytica Chimica Acta. 1022, 1-19.
DOI: https://doi.org/10.1016/j.aca.2018.02.080.

[25] Namsheer, K., Rout, C.S., 2021. Conducting polymers: a comprehensive review on recent advances in synthesis, properties and applications. RSC Advances. 11, 5659-5697.
DOI: https://doi.org/10.1039/d0ra07800j.

[26] Zhang, Y., Ye, J., Liu, Z., et al., 2020. Red-emissive poly(phenylene vinylene)-derivated semiconductors with well-balanced ambipolar electrical transporting properties. Journal of Materials Chemistry C. 8, 10868-10879.
DOI: https://doi.org/10.1039/d0tc01174f.

[27] Elacqua, E., Geberth, G.T., Vanden Bout, D.A., et al., 2019. Synthesis and folding behaviour of poly(p-phenylene vinylene)-based β-sheet polychromophores. Chemical Science. 10, 2144-2152.
DOI: https://doi.org/10.1039/c8sc05111a.

[28] Rodrigues, A.C.B., Geisler, I.S., Klein, P., et al., 2020. Designing highly fluorescent, arylated poly(phenylene vinylene)s of intrinsic microporosity. Journal of Materials Chemistry C. 8, 2248-2257.
DOI: https://doi.org/10.1039/c9tc06028f.

[29] Hsu, T.W., Kim, C., Michaudel, Q., 2020. Stereoretentive Ring-Opening Metathesis Polymerization to Access All- cis Poly(p-phenylenevinylene)s with Living Characteristics. Journal of the American Chemical Society. 142, 11983-11987.
DOI: https://doi.org/10.1021/jacs.0c04068.

[30] Zhang, H., Zhong, H., Dou, F., et al., 2021. Electrospinning bifunctional polyphenylene-vinylene/heated graphene oxide composite nanofibers with luminescent-electrical performance. Thin Solid Films. 725.
DOI: https://doi.org/10.1016/j.tsf.2021.138636.

[31] Ikizer, B., Lawton, C.W., Orbey, N., 2021. Poly (para-phenylene) fibers - Characterization and preliminary data for conversion to carbon fiber. Polymer (Guildf). 228, 123945.
DOI: https://doi.org/10.1016/j.polymer.2021.123945.

[32] Pavlović, D., Cohen, S., 2020. Controlled synthesis of unsubstituted high molecular weight poly(: Para -phenylene) via Suzuki polycondensation-thermal aromatization methodology. Polymer Chemistry. 11, 2550-2558.
DOI: https://doi.org/10.1039/d0py00001a.

[33] McBrearty, J., Barker, D., Damavandi, M., et al., 2018. Antimicrobial synergy of cationic grafted poly(para-phenylene ethynylene) and poly(para-phenylene vinylene) compounds with UV or metal ions against Enterococcus faecium. RSC Advances. 8, 23433-23441.
DOI: https://doi.org/10.1039/C8RA02673D.

[34] Lobo, L.S., Matsumoto, K., Jikei, M., et al., 2021. Hyperbranched Polyphenylene as an Electrode for Li-Ion Batteries. Energy Technology. 9, 1-7.
DOI: https://doi.org/10.1002/ente.202100374.

[35] Zhou, W.X., Cheng, Y., Chen, K.Q., et al., 2020. Thermal Conductivity of Amorphous Materials. Advanced Functional Materials. 30, 1-17.
DOI: https://doi.org/10.1002/adfm.201903829.

[36] Iqbal, S., Ahmad, S., 2018. Recent development in hybrid conducting polymers: Synthesis, applications and future prospects. Journal of Industrial and Engineering Chemistry. 60, 53-84.
DOI: https://doi.org/10.1016/j.jiec.2017.09.038.

[37] Han, Y., Dai, L., 2019. Conducting Polymers for Flexible Supercapacitors. Macromol. Chemical Physics. 220, 1-14.
DOI: https://doi.org/10.1002/macp.201800355.

[38] Tomczykowa, M., Plonska-Brzezinska, M.E., 2019. Conducting polymers, hydrogels and their composites: Preparation, properties and bioapplications. Polymers (Basel). 11, 1-36.
DOI: https://doi.org/10.3390/polym11020350.

[39] Yildiz, Z., Usta, I., Gungor, A., 2013. Investigation of the Electrical Properties and Electromagnetic Shielding Effectiveness of Polypyrrole Coated Cotton Yarns. Fibres & Textiles in Eastern Europe. 98, 32-37.

[40] Yildiz, Z., Usta, I., Gungor, A., 2012. Electrical properties and electromagnetic shielding effectiveness of polyester yarns with polypyrrole deposition. Textile Research Journal. 82, 2137-2148.
DOI: https://doi.org/10.1177/0040517512449046.

[41] Murugappan, K., Castell, M.R., 2018. Bridging electrode gaps with conducting polymers around the electrical percolation threshold. Electrochemistry Communications. 87, 40-43.
DOI: https://doi.org/10.1016/j.elecom.2017.12.019.

[42] Li, H., Lambert, C., Stahl, R., 2006. Conducting polymers based on alkylthiopyrroles. Macromolecules. 39, 2049-2055.
DOI: https://doi.org/10.1021/ma0601868.

[43] Zujovic, Z., Kilmartin, P.A., Travas-sejdic, J., 2020. Polymers. The Special Case on Polyaniline. Molecules. 25, 1-20.

[44] Wahane, D.S., Khobragade, Y.F., Gholse, S.B., et al., 2012. Synthesis and Structural Characterization of Polypyrrole / Metal Oxide Composite by NMR Spectroscopy. Journal Chemical Science. 2, 148-153.

[45] Hiragond, C.B., Khanna, P.K., More, P.V., 2018. Probing the real-time photocatalytic activity of CdS QDs sensitized conducting polymers: Featured PTh, PPy and PANI. Vacuum. 155, 159-168.
DOI: https://doi.org/10.1016/j.vacuum.2018.06.009.

[46] Xu, Y., Ma, Y., Ji, X., et al., 2019. Conjugated conducting polymers PANI decorated $Bi_{12}O_{17}Cl_2$ photocatalyst with extended light response range and enhanced photoactivity. Applied Surface Science. 464, 552-561.
DOI: https://doi.org/10.1016/j.apsusc.2018.09.103.

[47] Krishnaswamy, S., Ragupathi, V., Raman, S., et al., 2019. Optical properties of P-type polypyrrole thin film synthesized by pulse laser deposition technique: Hole transport layer in electroluminescence devices. Optik (Stuttg). 194, 163034.
DOI: https://doi.org/10.1016/j.ijleo.2019.163034.

[48] PuiggalÍ-Jou, A., Del Valle, L.J., Alemán, C., 2020. Encapsulation and Storage of Therapeutic Fibrin-Homing Peptides using Conducting Polymer Nanoparticles for Programmed Release by Electrical Stimulation. ACS Biomaterials Science & Engineering. 6, 2135-2145.
DOI: https://doi.org/10.1021/acsbiomaterials.9b01794.

[49] Poddar, A.K., Patel, S.S., Patel, H.D., 2021. Synthesis, characterization and applications of conductive polymers: A brief review. Polymers for Advanced Technologies. 32(2021), 4616-4641.
DOI: https://doi.org/10.1002/pat.5483.

[50] Prunet, G., Pawula, F., Fleury, G., et al., 2021. A review on conductive polymers and their hybrids for flexible and wearable thermoelectric applications. Materials Today Physics. 18, 100402.
DOI: https://doi.org/10.1016/j.mtphys.2021.100402.

[51] Wu, J.G., Chen, J.H., Liu, K.T., et al., 2019. Engineering Antifouling Conducting Polymers for Modern Biomedical Applications. ACS Applied Materials & Interfaces. 11, 21294-21307.
DOI: https://doi.org/10.1021/acsami.9b04924.

[52] Talikowska, M., Fu, X., Lisak, G., 2019. Application of conducting polymers to wound care and skin tissue engineering: A review. Biosens. Bioelectron. 135, 50-63.
DOI: https://doi.org/10.1016/j.bios.2019.04.001.

[53] Trojanowicz, M., 2003. Application of Conducting Polymers in Chemical Analysis. Microchimica Acta. 143, 75-91.
DOI: https://doi.org/10.1007/s00604-003-0066-5.

[54] Gereadr, M., Choubey, A., Malhotra, B., 2001. Review: Application of Conducting Polymer to Biosensors, Biosens. Bioelectron. 17, 345-359.

[55] Guo, X., Facchetti, A., 2020. The journey of conducting polymers from discovery to application. Nature Materials. 19, 922-928.
DOI: https://doi.org/10.1038/s41563-020-0778-5.

[56] Kraft, U., Molina-Lopez, F., Son, D., et al., 2020. Ink Development and Printing of Conducting Polymers for Intrinsically Stretchable Interconnects and Circuits. Advanced Electronic Materials. 6, 1-9.
DOI: https://doi.org/10.1002/aelm.201900681.

[57] Jeong, S.H., Kim, H., Park, M.H., et al., 2019. Ideal conducting polymer anode for perovskite light-emitting diodes by molecular interaction decoupling. Nano Energy. 60, 324-331.
DOI: https://doi.org/10.1016/j.nanoen.2019.03.030.

[58] Bilal, S., Farooq, S., Shah, A.U.H.A., et al., 2014. Improved solubility, conductivity, thermal stability and corrosion protection properties of poly(o-toluidine) synthesized via chemical polymerization. Synthetic Metals. 197, 144-153.
DOI: https://doi.org/10.1016/j.synthmet.2014.09.003.

[59] Tüken, T., Yazici, B., Erbil, M., 2005. Electrochemical synthesis of polythiophene on nickel coated mild steel and corrosion performance. Applied Surface Science. 239, 398-409.
DOI: https://doi.org/10.1016/j.apsusc.2004.06.006.

[60] Marzocchi, M., Gualandi, I., Calienni, M., et al., 2015. Physical and Electrochemical Properties of PEDOT:PSS as a Tool for Controlling Cell Growth. ACS Applied Materials & Interfaces. 7, 17993-18003.
DOI: https://doi.org/10.1021/acsami.5b04768.

BILINGUAL PUBLISHING CO.
Pioneer of Global Academics Since 1984

Organic Polymer Material Research
https://ojs.bilpublishing.com/index.php/opmr

ARTICLE

ATR-FTIR Analysis on Aliphatic Hydrocarbon Bond (C-H) Formation and Carboxyl Content during the Ageing of DC Air Plasma Treated Cotton Cellulose and Its Impact on Hydrophilicity

S. Anitha[1*] K. Vaideki[2]

1. Department of Basic Science (Physics), PSG Polytechnic College, Coimbatore, India
2. Department of Applied Science, PSG College of Technology, Coimbatore, India

ARTICLE INFO

Article history
Received: 8 April 2022
Revised: 18 May 2022
Accepted: 7 June 2022
Published Online: 14 June 2022

Keywords:
Cotton cellulose
DC air plasma process
Ageing of sample
Aliphatic hydrocarbon bond (C-H) formation
Carboxyl content

ABSTRACT

The surface of the cotton fabric was modified using a direct current (DC) air plasma treatment and hence enhances its hydrophilicity. The Box-Behnken approach (design expert software) was used to optimise the input process parameters. The sample prepared under optimized condition is subjected to ATR-FTIR and Field Emission Scanning Electron Microscopy (FESEM) studies in order to determine the changes in hydrogen bond energies (EH), Total Crystallinity Index (TCI), Hydrogen Bond Intensity (HBI), Lateral Order Index (LOI), functionalization, lattice parameters (a, b, c & β), degree of crystallinity (in %) and surface etching. The ageing of this sample has been studied by comparing the values of carboxyl content and AC-C/AC-O-C ratio calculated using data extracted from ATR-FTIR spectra of the sample recorded periodically for one month.

1. Introduction

Many researchers have reported the structure and the properties of the cotton fabric have been modified by plasma treatment. Plasma treatment of the cellulosic material modifies the surface thus changes the physical and chemical property of the fabric. Chemical and physical changes induce crystallinity changes, oxidation and etching of the sample. These physical and chemical modifications will enhance the wickability of cellulose materials after plasma treatment. In addition, when the fabric is subjected to plasma treatment carboxyl groups content present in the fabric increases thereby creates the channel for water penetration [1].

Fourier transform infrared spectroscopy and X-ray diffractogram are being increasingly used to carry out both qualitative and quantitative characterization of cellulose and cellulosic materials. Several articles on infrared spec-

**Corresponding Author:*
S. Anitha,
Department of Basic Science (Physics), PSG Polytechnic College, Coimbatore, India;
Email: vp.anitha@gmail.com

DOI: https://doi.org/10.30564/opmr.v4i1.4610

troscopy examination of native cotton have been published. FTIR spectroscopy is essential to obtain information about the hydrogen bonds and establish a relationship between the spectrum of hydroxyl groups and the crystallinity of cellulose [2].

Khai *et al.* (2017) [3] have explained the use of FTIR to evaluate the structural characteristic from the intensity of the characteristic bands. By comparing the peak of a functional group within crystalline domain with the peak of some other functional group in the amorphous domain in the FTIR analysis, the amount of crystalline and amorphous nature in cellulose can be determined. The shift and shape of the characteristic bands are used to research the transformation of cellulose structure.

O'Connor *et al.* (1958) [4] established the empirical "Crystallinity Index" for native cotton, wherein the authors explained the variation in a ratio-based crystallinity index absorption at 1429 cm^{-1} (CH_2 scissoring at C(6) in cellulose) and 893 cm^{-1} (C–O–C valence vibration of β-glycosidic link). Later, the authors (Nelson and O'Connor 1964b) [5], developed the absorption ratio at 1372 cm^{-1} (C–H deformation in cellulose) to 2900 cm^{-1} (C-H stretching) as the "Total Crystalline Index" to study the degree of crystallinity of cellulose.

Gaur *et al.* (2017) [6] related the degree of intermolecular regularity with the Hydrogen Bond Intensity (HBI). HBI of the cellulose sample are the proportion between the absorbance bands at 3400 cm^{-1} (H-bonded absorption) to 1320 cm^{-1} (CH_2 rocking vibration). The authors explained that the reason for reduction in HBI is due to the weakening or reorganization of H-bonds between glucan chains or inside the chain due to thermal treatments.

Poletto *et al.* (2014) [7] used FTIR spectroscopy in order to quickly learn about the structure of cellulose. The structural and chemical shifts in cellulose that occur as a result of different treatments have been correlated with Hydrogen Bond Intensity (HBI), Lateral Order Index (LOI) and Total Crystallinity Index (TCI) values.

M. El-Zawahry and N. A. Ibrahim (2006) [8] have carried out studies on the effect of ageing on Nitrogen plasma-treated wool fabric. It was noted that there is a a small reduction in the amount of acid dye uptake storage period of 100 hours which was ascribed resulting in the creation of additional anionic sites on the surface of the treated wool and as a result of anionic repulsion at the wool fibre surface, the electro negativity of the wool surface increases, and the tendency to absorb dye anions decreases. Another reason proposed by the authors was that because of the mobility of macromolecular segments, plasma-formed functional groups from the surface layer may be removed from the wool structure, reducing its ability to pick up dye anion.

N. Reza M.A. Malek and Ian Holme (2003) [9] studied the ageing process of cotton fiber after oxygen plasma treatment. The results show that during ageing process the oxidation of samples promoted more carboxyl groups on the fibres which would lead to higher electronegative surface potential. This leads to electrostatic repulsion of the direct dye anions and a decrease in the uptake of such a dye by the oxidized fibers.

In this line, this paper studies the impact of DC air plasma treatment on the surface oxidation and the hydrophilicity of cotton cellulose. ATR-FTIR spectroscopy is used to study the structural changes in cotton cellulose after the air plasma treatment. To evaluate the ageing process of treated cotton cellulose, the stability of free radicals formed on the surface of cotton cellulose as a result of air plasma modification was studied.

ATR-FTIR spectroscopy is employed to study the structural changes due to the plasma treatment and hence the increase in hydrophilicity due to structural changes. The evaluation of ageing process of DC air plasma modified cotton cellulose has been carried to study the stability of free radicals created on the cotton cellulose.

2. Experimental Methods

2.1 Cotton Fabric

Plain weave fabric made of 100 percent pure cotton with a warp count of Ne 22 and Ne 19's weft count was used in the current study. The EPI and PPI of the fabric are found to be 68 × 55, with the thickness of 0.36 mm and surface mass of 160 GSM. To remove starch, the cotton cloth was first soaked in boiling water for an hour and then air dried. Afterwards, the fabric was pressed on an industrial scale (Ironing).

2.2 DC Air Plasma Treatment

The electrodes and DC plasma chamber were made up of Stainless steel. The chamber was attached to the rotary pump, and the fabric sample of 20 cm × 20 cm was hooked between electrodes (Hind Hivac). In the presence of the fabric, the lowest possible base pressure was 0.2 millibar. The plasma chamber was shown in a schematic diagram in Figure 1.

Electrode gap, process gas pressure, DC current, and plasma exposure period were the process parameters that could be changed during plasma treatment. As a result, the parameters must be tweaked in order to achieve high hydrophilicity.

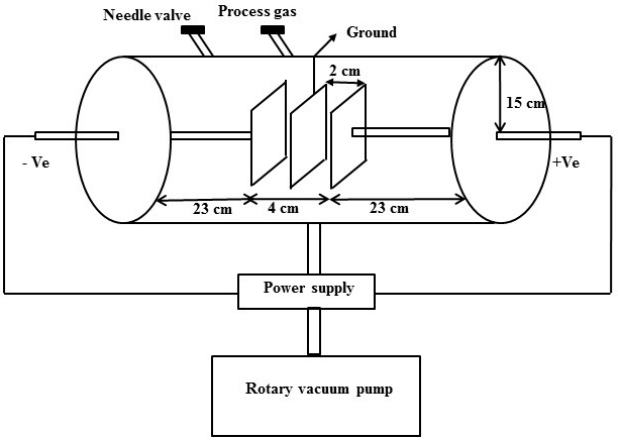

Figure 1. Schematic diagram of DC plasma chamber

2.3 Assessment of Hydrophilicity

The hydrophilicity of the untreated and DC air plasma treated samples was determined by employing the dynamic wicking test (BS 4554) to determine the wicking height (method of test for wettability of textile fabrics 1970). The average wicking height was determined by laying a strip of (2 cm × 20 cm) fabric vertically with its edge in contact with the distilled water and taking readings for five strips of the same sample. The rise in water level (wicking height) observed after 45 minutes was used to determine hydrophilicity.

The mean pore radius was determined using a modified Lucas Washburn equation and a dynamic wicking test (1) [10,11]. A graph is drawn between L^2 vs t, slope of the line gives the mean pore radius.

$$L^2 = \left(\frac{R\gamma}{2\eta}\right)t \tag{1}$$

where,
L – wicking height,
R – mean pore radius,
η – coefficient of viscosity of the liquid,
γ – surface tension of the liquid,
t – time taken for wicking.

2.4 ATR-FTIR Analysis

ATR-FTIR spectra were used to examine the chemical changes on the fabric surface caused by various procedures. A FTIR spectrometer (Perkin Elmer, USA, Spectrum Two) was used to capture the spectrum in the band of 4000 cm^{-1}~500 cm^{-1} with a 4 cm^{-1} resolution and 64 scans. The intensity values of peak heights were used to calculate the three standard crystallinity indices namely Hydrogen Bond Intensity (HBI), Total Crystallinity Index (TCI) and Lateral Order Index (LOI) described in literature [5,11]. IR spectral data was used to calculate the three indices, as well as hydrogen bond energy (E_H) and hydrogen bond distances (B_L).

The energy of hydrogen bonding (EH) was calculated using Struszczyk and Poletto's Equation (2) [7,12] as follows:

$$E_H = \frac{1}{k}\left(\frac{\nu_o - \nu}{\nu_o}\right) \tag{2}$$

where,
νo = standard frequency corresponding to free OH groups (3650 cm^{-1});
ν = frequency of the bonded OH groups;
k is a constant (1/ k = 2.625 × 10^2 kJ).

The hydrogen bond distances (B_L) for OH stretching bands was calculated using Equation (3) [7,13].

$$\Delta\nu\ (cm^{-1}) = 4430 \times (2.84 - B_L)$$
$$\Delta\nu = \nu_o - \nu \tag{3}$$

where,
ν_0 = monomeric OH stretching frequency, (3600 cm^{-1});
ν = stretching frequency observed in the infrared spectrum of the sample.

Lateral Order Index (LOI) proposed by Nelson and O'Connor [5] was used to evaluate the orderliness in cellulose and it was found using Equation (4).

$$\text{LOI} = \frac{A1430}{A898} \tag{4}$$

The IR spectra were used for the calculation of the Hydrogen Bond Intensity (HBI, A3400/A1320) proposed by (Nada *et al.* 2000) [14] and Total Crystallinity Index (TCI, A1372/A2900) proposed by (Nelson & O'Connor 1964) [5].
where,
A1430 - Intensity of A1430 cm^{-1} peak CH_2 scissoring at C_6 in cellulose;
A898 - Intensity of A898 cm^{-1} peak C-O-C valence vibration of β-glycosidic link;
A3400 - Intensity of 3400 cm^{-1} peak (O(2)H···O(6));
A1320 - Intensity of 1320 cm^{-1} peak (CH_2 wagging);
A1372 - Intensity of 1372 cm^{-1} peak (C–H deformation in cellulose);
A2900 - Intensity of 2900 cm^{-1} peak (CH_2 stretching in cellulose from C6).

2.5 FESEM Analysis

Etching and the creation of micro holes are two of the physical changes that the plasma treatment causes on the fabric surface. A Field Emission Scanning Electron Microscope was used to examine the surface morphology of the untreated and plasma-treated samples (Carl Zeiss, UK, SIGMA). The fabric samples were initially treated with

gold to prevent charging effects. Micrographs were taken at a magnification of 50000× for a 3 kV acceleration voltage.

2.6 Estimation of Concentration of Carboxyl Group-Sodium Bicarbonate-Sodium Chloride Test

The TAPPI (Technical Association of Pulp and Paper Industry) standard test for determining carboxyl group concentration in cotton fibres is the sodium bicarbonate-sodium chloride test [15]. The cotton sample is extracted with dilute hydrochloric acid in this process (0.1 M). The material is then filtered after being rinsed with distilled water and reacting with a 0.01 M sodium bicarbonate –0.1M sodium chloride solution. The filtrate is then titrated with 0.01 M hydrochloric acid while methyl red is used as an indicator. The formula is used to compute the carboxyl group concentration in meq/100 g.

Concentration of carboxyl group (meq/100 g)=

$$\left[B-\left(A+\frac{A\times C}{50}\right)\times M\times\frac{200}{W}\right] \quad (5)$$

where,

C - weight of water in wet fabric in grams;

W - oven dry weight of the sample in grams;

A - volume of 0.01 M HCl required to titrate 25 mL of the sample solution in mL;

M - Molarity of HCl used for titration;

B - volume of 0.01 M HCl required to titrate 25 mL of the sodium bicarbonate-sodium chloride original solution;

2 - factor for the used volume ratio between sodium bicarbonate-sodium chloride solution and filtrate used in the test;

50 - volume of sodium bicarbonate-sodium chloride solution used in the test.

3. Results and Discussions

The Box-Behnken design of experiment was used to optimise the parameters of the DC air plasma process. The optimization is carried out to attain the highest possible hydrophilicity in DC plasma treated samples for the parameters that have already been described in our earlier research [16]. The optimal process parameters for DC air plasma treatment are obtained when the gas pressure is 0.5 mbar, the treatment time is 15 minutes, and the DC current is 25 mA. The wicking response observed experimentally is 12.60 cm, compared to 9.4 cm for untreated fabric, indicating a (25 percent) increase in hydrophilicity.

The optimised sample is subjected to ATR-FTIR and FESEM analysis to study the structural and morphological changes of cellulose fabric surface due to DC air plasma treatment. Ageing analysis has been carried out for the optimised sample to ascertain the factors affecting the samples under stored conditions.

3.1 ATR-FTIR Analysis of Optimised Sample

To explore the effect of plasma surface modification in promoting capillarity action, the ATR-FTIR spectra of untreated (control) and plasma treated fabric (Figure 2) were compared. The spectral alterations after plasma therapy were compared to those described in the literature, and the results are shown in Table 1.

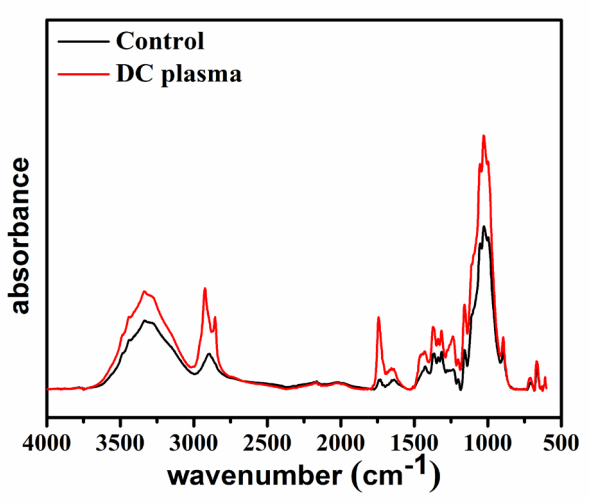

Figure 2. ATR-FTIR spectra of control and DC air plasma (optimised process parameters) treated sample

As discussed in earlier sections, the hydroxyl stretching region is crucial for understanding the hydrogen bonding systems. The OH stretching band covers 3-4 sub peaks i.e. the intermolecular hydrogen bond O6H···O3, intramolecular hydrogen bond O3H···O5 and O2H···O6 respectively. However, the bands corresponding to inter, intra and intersheet hydrogen bonds can only be noticed in the second derivative in most cases of the FTIR spectrum which the original data set does not allow for and hence deconvolution is used to determine the exact location of the peak of hydrogen bonds. This method of deconvolution enhances the resolution and even small difference in the spectrum can be identified. Similarly four sub peaks between 3000 cm^{-1} ~ 2800 cm^{-1} and 1740 cm^{-1} ~ 1710 cm^{-1} are identified by deconvolution method. The peak positions are discussed in the Table 1 and presented in the Figure 3 respectively.

The spectral changes in the above said peaks are discussed and related with the structural changes after plasma treatment.

Table 1. IR frequency of control and DC air plasma treated sample

Wavenumber (cm^{-1}) literature	Wavenumber (cm^{-1}) control fabric	Wavenumber (cm^{-1}) DC plasma treated fabric	Interpretation
3455–3410 (3420)	3456	3454	O2H···O6 intramolecular hydrogen bond in cellulose
3375–3340	3335	3339	O3H···O5 intramolecular hydrogen bond in cellulose
3310–3230	3255	3273	O6H···O3 intermolecular hydrogen bond in cellulose
2981–2933	2952	-	Asymmetric CH_2 valence vibration
2940–2850	2898 2870	2901 2874	Symmetric CH_2 valence vibration
2980–2835	2918 2853	2925 2856	Ring CH, CH_2,CH_2OH in cellulose from C6
1738–1709	1741 1728 1720 1710	1742 1730 1720 1712	C=O stretch in unconjugated ketones, carbonyls, esters.
1685–1655	1655	1655	C=O stretch
1636	1638	1638	Adsorbed water
1594 and 1558	-	1599	C=O stretch
1435	-	1431	H–O–C bending
1430–1416 (1420)	1425	1431	CH_2 scissoring at C(6) in cellulose
1376–1372 (1374)	1370	1370	C–H deformation in cellulose
1364	1364	1364	Symmetric C–H bending
1338–1335	1336	1338	O–H in-plain deformation
1316	1315	1316	CH_2 wagging
1282–1277	1261	1261	C–H deformation
1235–1225	1236	1237	O–H in-plain deformation at C(6)
1205–1200	1201	1202	O–H in-plain deformation
1162–1125 (1159)	1159	1159	C–O–C asymmetric from β-glycosidic link in cellulose
1110	1110	1110	Ring asymmetric valence vibration
1060–1015 (1170)	1053	1053	C–O vibration mainly from C(3)···O(3)H in cellulose II
1035–1030	1027	1027	C–O stretching
996–985	997	997	C–O valence vibration at C(6)
896–892 (899)	895	895	C–O–C valence vibration of β-glycosidic link
670–668	665	665	O–H out-of-plane bending

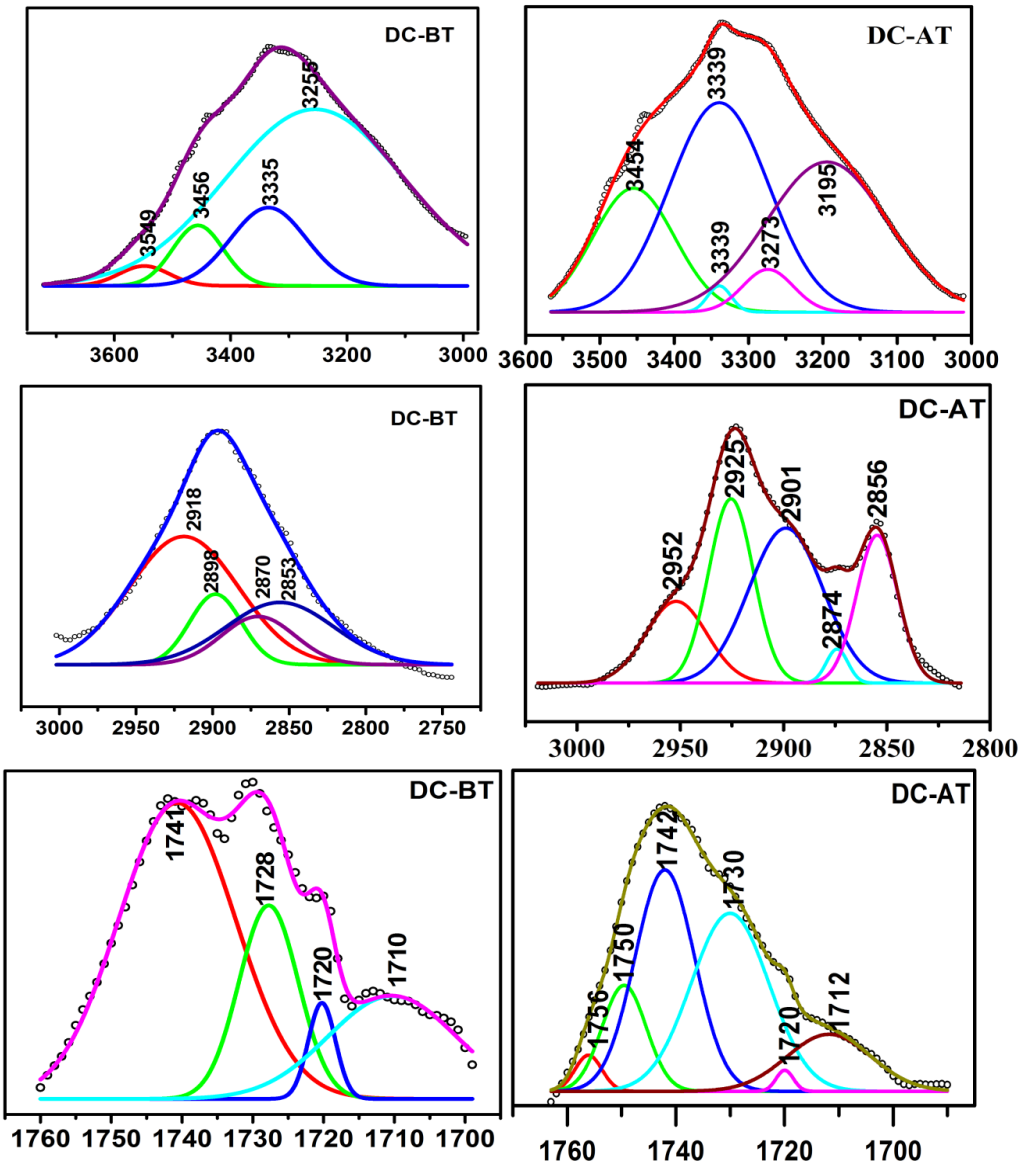

Figure 3. Deconvoluted spectra of control and DC air plasma (optimised process parameters) treated sample

The bond energies of hydrogen bond, LOI, TCI, HBI were calculated for the pre-treated and post treated samples and the results are presented in Table 2. Hence the increase in wicking ability has been discussed based on the results obtained.

In the unit cell of cellulose, the intermolecular hydrogen bond O6H···O3 lies along the

"b" axis, intramolecular hydrogen bonding O3H···O5, O2H···O6 which is parallel to glycosidic linkage C-O-C lies along "c" axis and the intersheet hydrogen bonding lies along "a" axis. Overall strains in the cellulose have been correlated with the wave number shift of intra and inter molecular hydrogen bonding. The shift in frequency of hydrogen bond changes the bond energy of the hydrogen bond and these changes induce strain in the cellulose promoting hydrophilicity.

It can be inferred from the Table 2, that the bond energies of all the hydrogen bond increases except for intramolecular hydrogen bond O2H···O6 decreases after DC air plasma treatment. The peak at 3255 cm^{-1} corresponding to O(6)H stretching (str) is shifted to 3273 cm^{-1} after plasma treatment that indicated an increase in bond energy of OH stretching and hence a decrease in bond length which resulted in the weakening of the O6H···O3 intermolecular hydrogen bond. Similarly the peak corresponding to C_6H_2 symmetric CH_2 valence vibration was shifted from 2898 cm^{-1} to 2901 cm^{-1} representing the shortening of the C-H bond which would result in the rotation of C5-C6 bond. The

Table 2. Hydrogen bond energy, LOI, TCI, HBI and intensity of acid groups of DC air plasma (optimised process parameters) treated sample

Bond energy and Bond length												
Process Parameters			**Intermolecular O6H···O3**		**Intramolecular O3H···O5**		**Intramolecular O2H···O6**		**Intersheet hydrogen bond (C – H···O)**		**Intersheet hydrogen bond (C – H···O)**	
P	**I**	**t**	**(3230-3310)**		**(3340-3375)**		**(3405-3460)**		**2920**		**2850**	
			ΔB_L (Å)	ΔE_H (kJ)	ΔB_L (Å)	ΔE_H (kJ)	ΔB_L (Å)	ΔE_H (kJ)	ΔB_L (Å)	ΔE_H (kJ)	ΔB_L (Å)	ΔE_H (kJ)
0.5	25	15	–0.0041	1.2945	–0.2877	0.0719	0.0005	–0.1438	–0.0016	0.5034	–0.0007	0.2158

TCI, LOI and HBI												
Process Parameters			**IR Crystallinity Ratio**			**Lateral order index**			**Hydrogen bond intensity**			**WH**
P	**I**	**t**	**TCI (A1372/A2900)**			**LOI (A1429/A893)**			**HBI (A3400/A1320)**			
0.5	25	15	0.71	0.47	0.24	0.57	0.41	0.16	3.23	1.67	1.56	12.60

Process parameters			**Physical and Chemical analysis**									
P	**I**	**t**	**WH (cm)**	**Intensity of C=O stretching**								
				Aldehyde				**Acid**				
				BT		**AT**		**BT**		**AT**		
				WN (cm^{-1})	Intensity (AU)	WN (cm^{-1})	Intensity (AU)	WN (cm^{-1})	Intensity (AU)	WN (cm^{-1})	Intensity (AU)
0.5	25	15	12.60	0.3364	1741	6.91E-3	1756 1750 1742 1730	0.01772 0.01953 0.04016 0.03246	1728 1720 1710	4.55E-3 2.29E-3 2.42E-3	1720 1712

BT-Before treatment, AT-After treatment, WN-Wave number

rotation of the C5-C6 covalent bond will again affect the intermolecular hydrogen bond [17,18]. Considering the intramolecular hydrogen bond, a shift in 3335 cm^{-1} (O3H str) to 3339 cm^{-1} and 3456 cm^{-1} (O2H str) to 3454 cm^{-1} respectively is observed. This results in lengthening of O3H···O5 intramolecular hydrogen bond and shortening of the O2H···O6 [17,18]. Another finding from the ATR-FT-IR spectra is that following plasma treatment, the peak at 2853 cm^{-1} (ring C-H stretching) [17] vibrations is shifted to higher frequency 2856 cm^{-1}, indicating that the C-H covalent bond is strengthened and the inter sheet CH···O bond is weakened. The cellulose unit cell experiences strain as a result of these general changes in the hydrogen bond. The overall changes induced in the cellulose are shown in Figure 4.

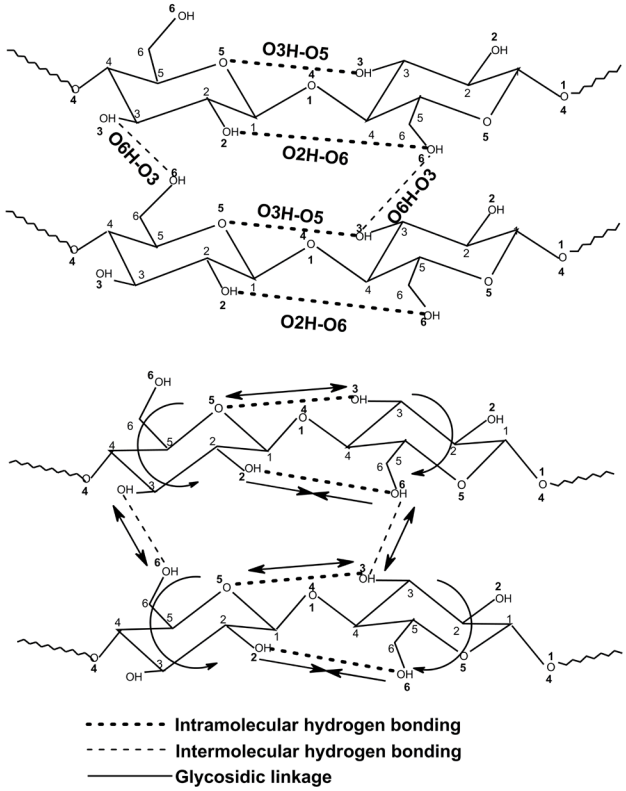

Figure 4. Structural changes due to DC air plasma treatment using optimised process parameters

The weakening of hydrogen bonds has been correlated with the values of LOI, TCI and HBI. It is noted from the Table 2, all the calculated values decrease with plasma treatment which implies that there is a decrease in crystallinity of cellulose. These changes after plasma treatment generate free hydroxyl groups. These accessible hydroxyl groups are easily prone to oxidation when in contact with the plasma species. This has been confirmed from the spectral range between 1740 cm^{-1} to 1710 cm^{-1} where the increase in intensity of C=O peak has been observed after plasma treatment. The four possible sites for oxidation in a cellulose molecule are C_1, C_2, C_3 and C_6 [19,20].

McCord *et al.* (2003); Ward *et al.* (1979) [19,20] have suggested five possible oxidation mechanisms that are as follows: (i) bond breakage between C_1 and glycosidic bond oxygen, (ii) dehydrogenation and dehydroxylation between C_2 and C_3 after the ring opening of anhydroglucose, (iii) bond breakage between C_1 and ring oxygen (iv) dehydrogenation at C_6, (v) dehydroxylation at C_6, bond breakage between C_1 and ring oxygen. The peaks corresponding to 1157 cm^{-1} and 895 cm^{-1} in both spectra are identical in strength, confirming the absence of chain scission or ring opening, as shown in Figure 2 and hence oxidation doesn't occur at C_1, C_2 and C_3 sites. Hence it has been confirmed that oxidation is due to dehydrogenation at C_6. Increase in intensity of C=O peaks implies that more polar groups have been generated and hence there is an increase in hydrophilicity.

3.2 FESEM Analysis of Optimised Sample

A scanning electron microscope is used to examine the surface morphology of control and DC air plasma treated samples. Figure 5 shows FESEM micrographs of untreated and DC air plasma treated cotton fabric at magnifications of 250× and 50000× respectively.

It can be shown that when energetic charged particles in the plasma interact with the fabric, they cause not only chemical and structural changes on the sample surface, but also physical changes such as increase in the existing pore dimension, etching and the formation of micro cavities. By comparing the surface morphology and pore size of the untreated and plasma-treated samples, these alterations can be explained.

The FESEM micrograph of untreated (control) fabric of 250× magnification elucidate that the voids between the warp and weft in the fabric are not open. There are a lot of fibers running across the voids present between the warp and the weft. It is clear from the Figure 5, that the plasma treatment removes the thin hair like fibers running across the warp and weft increasing the void space between warp and weft. The etching of fiber surface after plasma treatment is also evident from Figure 5.

The increase in pore dimension has been quantified by calculating mean pore radius (Table 3) using modified Lucas Washburn Equation (1).

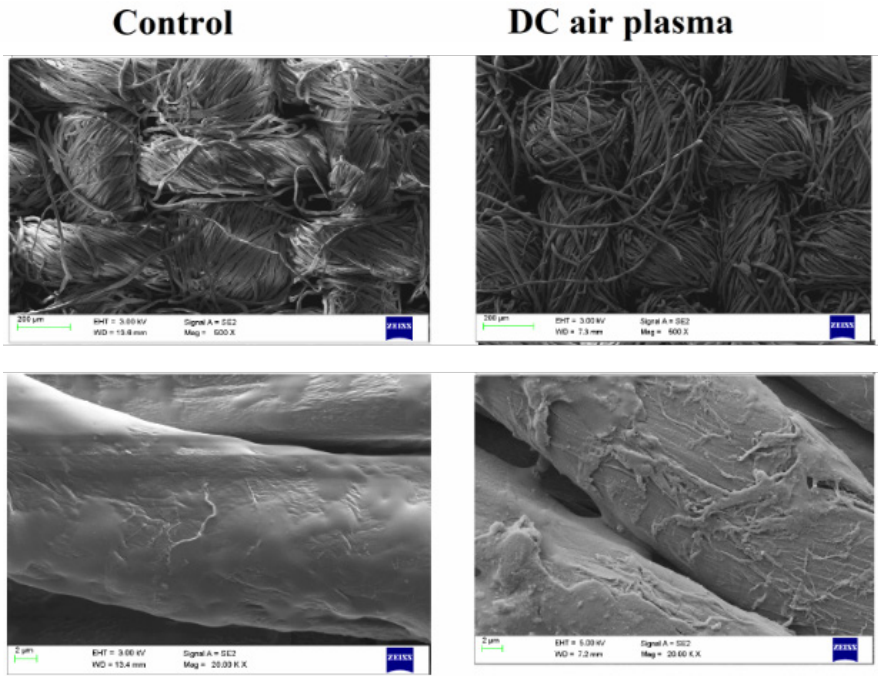

Figure 5. FESEM micrographs of control and DC air plasma (optimised process parameters) treated fabric

Table 3. Mean pore radius of control and DC air plasma (optimised process parameters) treated sample

Sample	Mean pore radius (μm)
Control (untreated)	0.117
DC plasma treated sample	0.336

The results of mean pore radius suggest that bombarding the fabric surface with plasma particles raises the mean pore size, improving the capillarity of cotton fabric and thus enhancing the fabric's hydrophilicity. These findings are consistent with those of Pandiyaraj and Selvarajan (2008) [21].

3.3 Ageing Analysis of DC Air Plasma Treated Cotton Fabric

Investigations are carried out on ageing of plasma treated samples. The wicking height of fabric depends on the concentration of carboxyl content. The wicking ability of the sample increases with increase in carboxyl content and hence plasma treatment promotes oxidation and this leads to an increase in concentration of carboxyl group which was tabulated in Table 4. Even though the plasma treatment improves hydrophilic nature of the fabric, it is necessary to analyze the ageing effect of the fabric. Hence the wicking ability of the samples stored in open air was measured after a week and a month period. In addition, the quantification of carboxyl content and ATR-FTIR analysis was carried out in order to validate the results of variation in wicking height.

The concentration of carboxyl group has increased in DC air plasma treated cotton samples after a seven-day and one-month ageing period, as shown in the Table 4. Upon ageing, the free radicals formed due to plasma treatment react with oxygen in the atmospheric air in turn generates more carbonyl and carboxyl groups leading to oxidation of primary hydroxyl groups on the surface of the fabric [22]. Figure 6 shows an increase in the intensity of peaks at 1740 cm^{-1}~1710 cm^{-1} corresponding to C=O stretching, which confirms the oxidation process.

Table 4. Ageing analysis of DC air plasma treated cotton cellulose

Sample	DC Plasma Treatment			
	WH (cm)	Carboxyl content meq/100 g	Absorbance ratio $\frac{\text{C-C}}{\text{C-O-C}}$	Intensity of Ring CH stretching
Control	9.20	1.561	1.698	1.200E-3
On the day of plasma treatment	12.60	1.613	1.817	5.395E-4
One week after ageing period	11.90	1.701	1.976	1.078E-3
One month after ageing period	10.80	2.137	2.085	6.144E-4

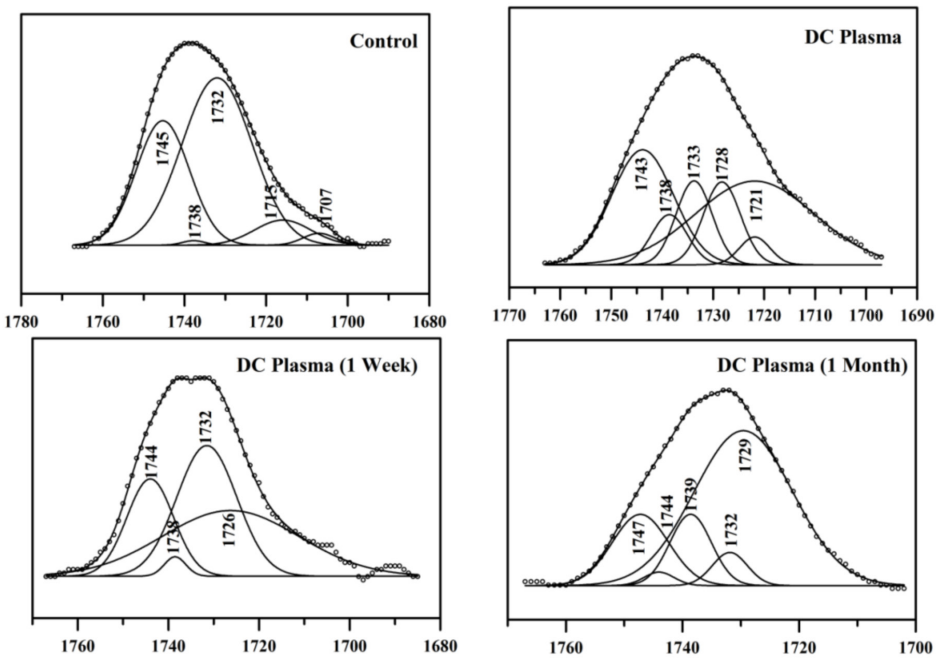

Figure 6. Deconvolution of C=O peaks for DC air plasma treated sample

The increase in carboxyl content concentration due to ageing develops an electronegative potential on the fabric surface which repel the anions through electrostatic repulsion phenomenon thereby decreasing the water uptake capacity [23].

Another possibility might be due to surface reversibility which could be due to either surface reorientation of low molecular weight oxidized materials (LMWOM) into bulk polymer or the reaction of free radicals with new groups or the environment [24]. However, from the IR spectra it can be observed that there was a significant increase in absorbance ratio of $\frac{\text{c-c}}{\text{c-o-c}}$ (Table 4) which is related to the concentration of the C-C component.

The absorbance ratio was determined by dividing the absorbance of C-C band frequency, i.e. 1100 cm^{-1} by absorbance of C-O-C frequency (glycosidic bond, 1158 cm^{-1}) which was used as an internal reference. Parallely, a slight decrease in concentration of ring CH (2850 cm^{-1}) was observed which is evident from the Table 4 and Figure 7.

The increase in absorbance ratio and decrease in concentration of ring CH reveals the fact that with ageing the formation of aliphatic carbon- carbon single bond increases.

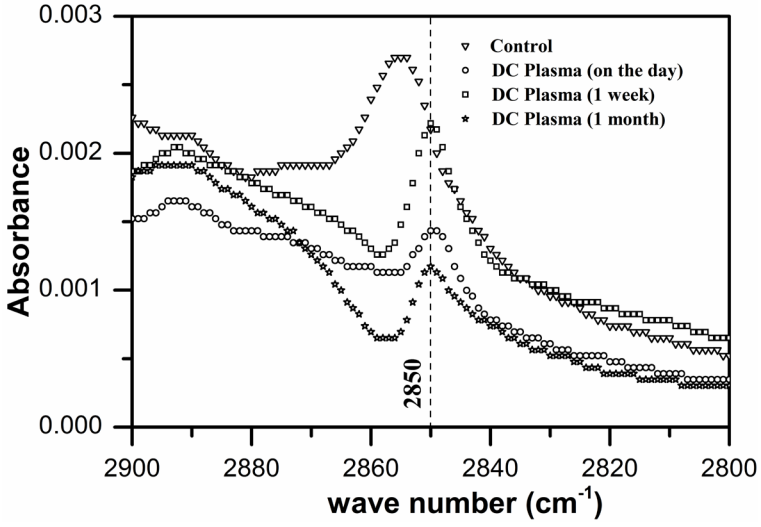

Figure 7. Ageing analysis with reference to the concentration of ring CH

This might be due to the reaction of free radicals with the ambient environment which leads to the transformation of surface polarity. During plasma treatment, reactive species such as H^+ and H^{2+} in the gas mixture bombard the surface of the fabric. As a result, the free radicals are formed on the surface of the fabric by eliminating an atom from a saturated compound as shown in Equation (6) and these free radicals on the polymer chain combines together [25] as shown in Equation (7).

$$-C\text{-}C\text{-}H + H^+ \longrightarrow -C\ -C\ + H_2^+ \quad (6)$$

$$2\text{-}C\text{-}C \longrightarrow -\ C\text{-}C\text{-}C\text{-}C\text{-} \quad (7)$$

The Equation (6) reveals the formation of free radicals on the fabric surface when subjected to plasma treatment and this has been substantiated through IR analysis wherein, decrease in concentration of ring CH is observed which indicates the formation of free radicals in the cellulose chain. These free radicals combine with the radicals which are generated on the neighbouring chain to form carbon-carbon single bond during storage period as depicted in Equation (6). These bonds hinder the diffusion of water through the surface. The formation of aliphatic hydrocarbon has been proved in IR analysis with increase in absorbance ratio of $\frac{\text{C-C}}{\text{C-O-C}}$. Thus with ageing effect, wettability of the fabric decreases because of the cross links.

Thus the ageing studies reveal that the cellulose structure is affected drastically upon storage, emphasizing that any post treatments should be immediately carried out after the plasma treatment.

4. Conclusions

The cotton fabric was treated with DC air plasma to modify the fabric's surface and the process parameters were optimised using the Box-Behnken design to obtain maximal wicking response. The samples were treated with plasma under optimised conditions suggested by the software and the structural and morphological changes have been analyzed using FESEM and ATR - FTIR studies. The ATR-FTIR study demonstrates the formation of free OH groups due to weakening of intermolecular and intramolecular hydrogen bonds that hold the chain together. This is reflected in the decrease in LOI, HBI and TCI values. Further, the generated free hydroxyl group oxidized to form new carboxylic acid (C=O) peaks which are more polar in nature. DC plasma treatment improves the capillary action by etching process. Due to the DC air plasma treatment, these alterations were caused on the fabric to enhance the hydrophilic nature of the fabric. FESEM analysis confirms the surface roughness and size of micro cavities in the fabric have increased as a result of the DC plasma treatment.

Ageing effect of plasma treated samples was investigated and it was noted that the aged samples were oxidized due to exposure to open atmosphere which was ascertained through carboxyl test and IR analysis. The increased carboxyl content decreases the wickability due to two possible mechanisms (i) electronegative potential developed on the surface repels the anions thereby decreasing the water uptake capacity and (ii) reversibility of surface polarity due to free radical formation which promoted the formation of C-C bonds thereby decreasing the wickability. Thus the ageing studies indicate that the plasma pretreated fabric has to be immediately processed for further studies.

Acknowledgements

The authors wish to thank the Management and Principal, PSG College of Technology, Coimbatore for providing the necessary infrastructure to carry out the study.

Conflict of Interest

There is no conflict of interest.

References

[1] Prabhakaran, M., Carneiro, N., 2005. Effect of low temperature plasma on cotton fabric and its applications to bleaching and dyeing. Indian Journal of Fibre Textile Research. 30, 68-74.

[2] Lee, C.M., Kubicki, J.D., Fan, B., et al., 2015. Hydrogen-bonding network and OH stretch vibration of cellulose: comparison of computational modeling with polarized IR and SFG spectra. The Journal of Physical Chemistry B. 119(49), 15138-15149.

[3] Khai, D.M., Nhan, P.D., Hoanh, T.D., 2017. An investigation of the structural characteristics of modified cellulose from acacia pulp. Vietnam Journal of Science and Technology. 55(4), 452-460.

[4] O'Connor, R.T., DuPré, E.F., Mitcham, D., 1958. Applications of infrared absorption spectroscopy to investigations of cotton and modified cottons: Part I: Physical and crystalline modifications and oxidation. Textile Research Journal. 28(5), 382-392.

[5] Nelson, M.L., O'Connor, R.T., 1964. Relation of certain infrared bands to cellulose crystallinity and crystal lattice type. Part II. A new infrared ratio for estimation of crystallinity in celluloses I and II. Journal of Applied Polymer Science. 8(3), 1325-1341.

[6] Gaur, R., Semwal, S., Raj, T., et al., 2017. Intensification of steam explosion and structural intricacies impacting sugar recovery. Bioresource Technology.

241, 692-700.

[7] Poletto, M., Ornaghi, H.L., Zattera, A.J., 2014. Native cellulose: structure, characterization and thermal properties. Materials. 7(9), 6105-6119.

[8] El-Zawahry, M.M., Ibrahim, N.A., Eid, M.A., 2006. The Impact of Nitrogen Plasma Treatment upon the Physical-Chemical and Dyeing Properties of Wool Fabric. Polymer-Plastics Technology and Engineering. 45(10), 1123-1132.
DOI: https://doi.org/10.1080/03602550600728943

[9] Malek, R.M., Holme, I., 2003. The effect of plasma treatment on some properties of cotton. Iranian Polymer Journal. 12, 271-280.

[10] Kalogianni, E.P., Savopoulos, T., Karapantsios, T.D., et al., 2004. A dynamic wicking technique for determining the effective pore radius of pregelatinized starch sheets. Colloids and Surfaces B: Biointerfaces. 35(3-4), 159-167.

[11] Pandiyaraj, K.N., Selvarajan, V., 2008. Non-thermal plasma treatment for hydrophilicity improvement of grey cotton fabrics. Journal of Materials Processing Technology. 199(1-3), 130-139.

[12] Struszczyk, H., 1986. Modification of lignins. III. Reaction of lignosulfonates with chlorophosphazenes. Journal of Macromolecular Science—Chemistry. 23(8), 973-992.

[13] Pimentel, G.C., Sederholm, C.H., 1956. Correlation of infrared stretching frequencies and hydrogen bond distances in crystals. The Journal of Chemical Physics. 24(4), 639-641.

[14] Nada, A.A.M., Kamel, S., El-Sakhawy, M., 2000. Thermal behaviour and infrared spectroscopy of cellulose carbamates. Polymer Degradation and Stability. 70(3), 347-355.

[15] TAPPI Standards: Regulations and Style Guidelines, 1977. https://www.tappi.org/globalassets/documents/standards/tm_guidelines_complete.pdf. Carboxyl Content of Pulp, T 237 os-77, 1-7.

[16] Anitha, S., Vaideki, K., Prabhu, S., et al., 2019. ATR-FTIR analysis on the hydrogen bonding network and glycosidic bond of DC air plasma processed cellulose. Journal of Molecular Structure. 1180, 378-391.

[17] Altaner, C.M., Horikawa, Y., Sugiyama, J., et al., 2014. Cellulose I_β investigated by IR-spectroscopy at low temperatures. Cellulose. 21(5), 3171-3179.

[18] Nishiyama, Y., Langan, P., Chanzy, H., 2002. Crystal structure and hydrogen-bonding system in cellulose I_β from synchrotron X-ray and neutron fiber diffraction. Journal of the American Chemical Society. 124(31), 9074-9082.

[19] McCord, M.G., Hwang, Y.J., Qiu, Y., et al., 2003. Surface analysis of cotton fabrics fluorinated in radio-frequency plasma. Journal of Applied Polymer Science. 88(8), 2038-2047.

[20] Ward, T.L., Jung, H.Z., Hinojosa, O., et al., 1979. Characterization and use of radio frequency plasma-activated natural polymers. Journal of Applied Polymer Science. 23(7), 1987-2003.

[21] Pandiyaraj, K.N., Selvarajan, V., 2008. Non-thermal plasma treatment for hydrophilicity improvement of grey cotton fabrics. Journal of Materials Processing Technology. 199(1-3), 130-139.

[22] Golova, O.G.P., Nosova, N.I., 1973. Degradation of cellulose by alkaline oxidation. Russian Chemical Reviews. 42(4), 327-333.

[23] Malek, R.M., Holme, I., 2003. The effect of plasma treatment on some properties of cotton. Iranian Polymer Journal. 12, 271-280.

[24] Kolářová, K., Vosmanská, V., Rimpelová, S., et al., 2013. Effect of plasma treatment on cellulose fiber. Cellulose. 20(2), 953-961.

[25] Kan, C.W., Yuen, C.W.M., 2006. Low Temperature Plasma Treatment for Wool Fabric. Textile Research Journal. 76, 309-314.

BILINGUAL PUBLISHING CO.
Pioneer of Global Academics Since 1984

Organic Polymer Material Research
https://ojs.bilpublishing.com/index.php/opmr

REVIEW

Chitosan-based Nanosystems as Drug Carriers

R. Yu. Milusheva* **S. Sh. Rashidova**

Institute of Polymer Chemistry and Physics, Academy of Sciences, Tashkent Kadyri 76, Tashkent, 100128, Uzbekistan

ARTICLE INFO

Article history
Received: 20 April 2022
Revised: 27 May 2022
Accepted: 22 June 2022
Published Online: 4 July 2022

Keywords:
Chitosan
Nanochitosan
Modification
Nanoparticle synthesis
Chemical structure
Ionotropic gelation
Covalent crosslinking

ABSTRACT

The formation and application of polymeric nanomaterials is great demand in science, industry, biotechnology, and medicine due to the possibility of achieving a significant improvement in the physicochemical, mechanical, and barrier properties of polymers and using them as drug carriers and fillers, which is especially promising for biodegradable polymers such as chitosan and their derivatives. The article presents methods for creating polymer nanostructures based on polysaccharides and, in particular, chitosan. Obtaining nanostructured samples of chitosan using the approaches of chemical transformation and modification of polysaccharides is an urgent scientific problem, the solution of which makes it possible to obtain new polymer systems of great practical interest. The medical aspects of the use of polymer carriers based on chitosan for the treatment of various diseases are discussed. The unique specificity of the properties of chitosan and nanomaterials derived from it, with the properties inherent in this natural polymer, can serve as a promising future, especially in the field of medicine.

1. Introduction

The creation of polymeric nanomaterials with specific properties in the last decade has been used in various industries, innovative technologies for the production of modern drugs, since it is so far the only way to synthesize unique drugs based on biodegradable polymers, which include chitosan. Of particular interest is the establishment of the relationship between the conditions for the synthesis and formation of nanopolymer systems based on chitosan and the identification of their correlation with biological activity. The study of the possibility of forming NP nanoparticles from natural polymers (polysaccharides) - chitosan and its derivatives under the influence of chemical and physical factors, the functionalization and stabilization of polysaccharide nanoparticles, the assessment of their structure and properties by physicochemical methods is relevant for modern polymer chemistry.

Obtaining nanostructured samples of chitin, chitosan using the approaches of chemical transformation and modification of polysaccharides is an urgent scientific problem, the solution of which makes it possible to obtain

**Corresponding Author:*
R. Yu. Milusheva,
Institute of Polymer Chemistry and Physics, Academy of Sciences, Tashkent Kadyri 76, Tashkent, 100128, Uzbekistan;
Email: rumilusheva@gmail.com

DOI: https://doi.org/10.30564/opmr.v4i1.4644

new polymer systems of great practical interest.

One of the promising materials for creating drug delivery systems is chitosan, a deacetylated derivative of the natural polysaccharide chitin. Chitosan is practically the only polycation of natural origin, which is characterized by low immunogenicity. Chitosan is non-toxic, biocompatible, and also biodegradable, which eliminates the possibility of its accumulation in the human body and the environment. Therefore, the synthesis of mixtures based on chitosan and synthetic polymers, as well as the inclusion of drugs in these mixtures, the study of the features of their molecular and supramolecular organization and various external influence factors, is necessary to obtain polymer nanomaterials with unique properties.

Such structures have a high affinity for the cell membrane and are small in size, which makes it easy to penetrate into the cell nucleus. These studies will contribute to the development of polymer nanomaterials with fundamentally new performance indicators.

2. Characterization of Chitosan Nanoparticles

It is generally accepted that nanoparticles are referred to as submicron, colloidal particles having one size less than 100 nm. For the first time, information about polymer nanoparticles was discussed in the article [1], which led to a boom in research for the development of polymer nanocarriers for drug delivery.

Ultra-small sizes of nanoparticles allow them to purposefully deliver drugs to the desired organs [2]. Nanoparticles based on chitosan and polyethyleneimine (PEI) have been studied for the delivery of anticancer drugs.

These nanoparticles can be broadly divided into:

(1) nanospheres are spherical particles in which the drug is inside the sphere, or on the outer surface, or both options are combined;

(2) nanocapsules - consist of an inner liquid core with a solid polymer shell, drugs are located inside the core, or on the outer surface, or both (Figure 1).

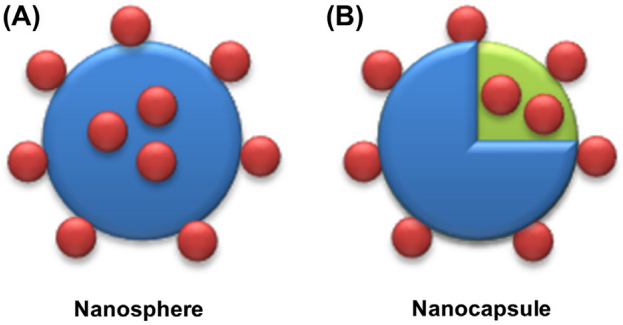

Figure 1. (A). Nanospheres, (B) Nanocapsules

Nanoparticles are of various shapes: cylinders, nanorods, nanotubes, cones, spheres, etc. [3].

Chitosan, a derivative of chitin, is a heteropolymer consisting of N-acetylglucosamines and b-(1,4)-linked glucosamine residues. Chitosan is synthesized by alkaline N-deacetylation of chitin at elevated temperature (Figure 2).

The properties of chitosan are due to its chemical structure. The formation of nanoparticles based on chitosan can serve as one of the ways to modify it. Chitosan molecules contain amino groups, which are partially protonated in slightly acidic aqueous solutions, and completely protonated at pH = 4. Thus, the chitosan molecule in solution is present in the cationic polyelectrolyte form, which opens up wide opportunities for interaction with negatively charged molecules: anions and polyanions. The choice of a simple and affordable method for the synthesis of nanoparticles from a specific chitosan derivative requires careful selection of conditions.

Modification of chitin under controlled conditions makes it possible to obtain chitosan with a degree of deacetylation (DDA) up to 98% and a molecular weight (M_W) from 5×10^4 Da to 2×10^6 Da. The physicochemical and biological properties of chitosan are directly dependent on DDA and the degree of polymerization (DP), on the basis of which the molecular weight of the polymer is determined. The study of the chemical structure shows

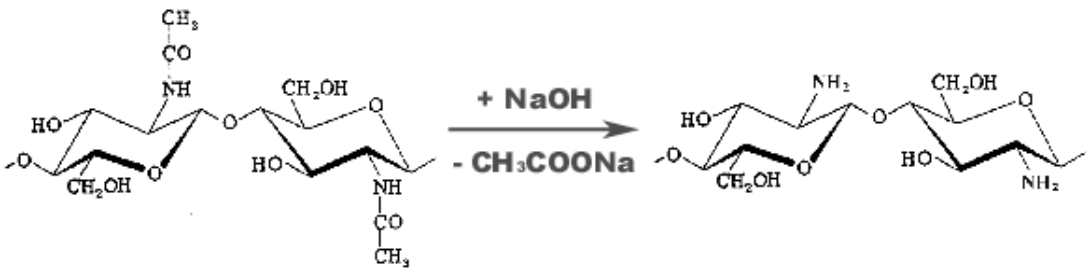

Figure 2. N-deacetylation of chitin to chitosan

that chitosan has reactive hydroxyl and amino groups. Chitosan is an amorphous polymer, unlike chitin, which has a crystalline structure. The presence of primary amino groups in chitosan with a pKa value of 6.3 makes it possible to classify it as a strong base [4].

At a pH above 6, chitosan loses its charge and solubility, since the amino groups are deprotonated at this pH. At a lower pH, the amino groups are protonated and become positively charged, providing chitosan with water solubility, which allows it to be classified as a cationic polyelectrolyte. In the pKa range between 6 and 6.5, there is a transition between solubility and insolubility. Therefore, chitosan dissolves well in a weak acid medium: acetic acid, hydrochloric acid, and does not dissolve at neutral and alkaline pH values. In addition to pH, the solubility of chitosan is highly dependent on DDA, M_W and the ionic strength of the solution. Under physiological conditions, chitosan can be easily degraded by lysozymes or chitinases, which are products of the normal flora in the human intestine or exist in the blood [5-7]. With an optimal N/P ratio (ratio of amino nitrogen in chitosan/ to DNA phosphate), chitosan can efficiently adsorb DNA to form nanoparticles with sizes that allow penetration into the cell, thus providing protection against enzymatic degradation of nuclease [8]. Due to these properties, chitosan is considered a biodegradable, biocompatible polymer and is widely studied as a matrix for drug delivery [9-15]. Since chitosan nanoparticles (CP chitosan) are currently widely used as nanocarriers for drugs, it is necessary to compare different methods for the preparation and characterization of chitosan nanoparticles.

3. Methods for Obtaining Chitosan Nanoparticles

There are several methods for obtaining chitosan nanoparticles of various sizes according to their further application:

1) Polyelectrolyte complex formation - occurs during electrostatic interaction between an anion and cation, followed by charge neutralization, NPs with a size of 50 nm~700 nm are formed;

2) Ionotropic gelation - using a cross-linking agent such as sodium tripolyphosphate (Na-TPP), the NP size can be adjusted depending on the reaction conditions;

3) Microemulsion method - nanoparticles are formed in the liquid phase of a reverse micelle using a surfactant and a crosslinking agent - nanoparticles smaller than 100 nm;

4) Covalent crosslinking - nanoparticles obtained by covalent crosslinking between chitosan and crosslinking agents, such as PEG, glutaraldehyde, etc., produce nanoparticles of various sizes;

5) Combination and incubation - This method allows you to mix the protein with chitosan, with mandatory washing in a mixture with Na-TPP, the formation of NPs with a size of 100 nm~150 nm;

6) Evaporation of the solvent - adding chitosan to an aqueous medium with the formation of an emulsion and precipitation, then evaporation is carried out, NPs with sizes of 50 nm~300 nm are obtained;

7) Co-precipitation - co-precipitation of a solution of chitosan obtained in a solution of CH_3COOH with a low pH by adding to a solution with a high pH of 8.5-9.0 (ammonium hydroxide solution) with the formation of highly monodispersed NPs up to 10 nm in size.

8) Complex coacervation - NPs are obtained by coacervation between cationic chitosan and anionic polyanions, polymers or biomacromolecules. The NP size depends on the anionic coacervate used.

3.1 Method of Polyelectrolyte Complex Formation

The formation of a polyelectrolyte complex (PEC) occurs due to the electrostatic interaction between the anion and the cation, followed by charge neutralization (Figure 3).

Due to charge neutralization, the polyelectrolyte complex self-organizes, which leads to a decrease in hydrophilicity. The formed nanocomplexes can have different sizes from 50 nm to 700 nm.

These polyelectrolyte complexes are used as carriers for proteins, peptides, drugs, and plasmid DNA.

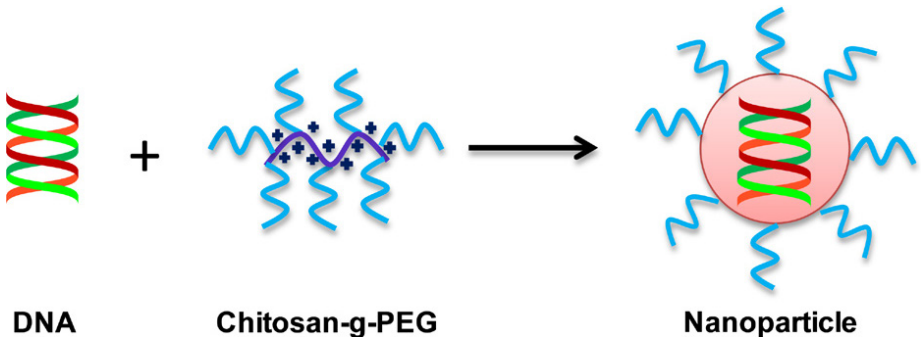

Figure 3. The method of polyelectrolyte complex formation: the formation of nanoparticles occurs during the electrostatic interaction of an anion (DNA) with a cation (chitosan) during charge neutralization.

The authors of the research [16] obtained chitosan-dextran nanoparticles by the method of polyelectrolyte complex formation with a size of 300 nm~500 nm and a zeta potential of + 40 mV~50 mV. Chitosan and dextran nanocomplexes can be used as effective delivery systems.

Another study was also carried out by the method of polyelectrolyte complex formation with the preparation of water-soluble chitosan nanocarriers for insulin [17]. The nanoparticles obtained by the method described above were about 200 nm in size.

Under simple and mild conditions, heparin and chitosan NPs were prepared by polyelectrolyte complexation [18]. The influence of pH, M_w, and concentration was studied when obtaining nanoparticles of the desired size and their yield. It has been shown that effective complex formation occurs at a lower pH and average molecular weight.

3.2 Ionotropic Gelation Method

The method of ionotropic gelation of chitosan nanoparticles was used with the help of ionic crosslinking agents [19]. Crosslinking occurs when intermolecular or cross-links are formed between polysaccharide molecules. Crosslinking sharply reduces the mobility of segments in the polymer with the formation of new interchain bonds and the formation of a three-dimensional network. At a high degree of crosslinking, the polymer matrix becomes insoluble both in water and in organic solvents [20]. Crosslinkers are broadly classified based on the interaction of crosslinkers with chitosan during crosslinking. There is physical and chemical crosslinking.

When physically crosslinked, polysaccharides form a network with counterions on the surface. A high counterion concentration requires a longer time for complete crosslinking of the polysaccharide. This method makes it possible to obtain reversible nanoparticles that are biocompatible due to the absence of harsh conditions for obtaining. Ionically crosslinked nanoparticles are typically pH sensitive, which is a prerequisite for controlled release. Ionic crosslinking occurs using sodium tripolyphosphate (Na-TPP), sulfuric acid, inorganic ions such as Fe $(CN)_6^4$, Fe $(CN)_6^3$ citrate, and calcium ions as crosslinkers [21].

An available and widely used method for obtaining chitosan nanoparticles is the ionotropic gelation of chitosan with sodium tripolyphosphate (Na-TPP), which has a triple negative charge in the physiological pH range.

During the preparation of chitosan nanoparticles using tripolyphosphate (TPP), the average size of NPs and their storage stability were controlled, and it was studied how these parameters are affected by the polymer concentration, the ratio of components, and other parameters.

Figure 4 is a diagram showing the interaction of positively charged chitosan chains with a negatively charged tripolyphosphate anion.

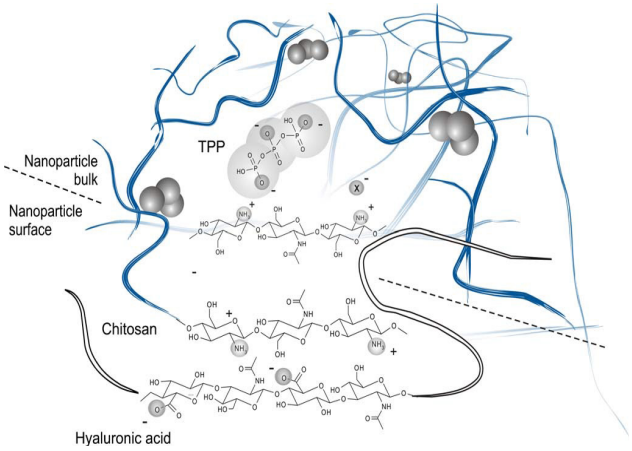

Figure 4. Graphical view of chitosan/TPF nanoparticles present in the volume of NPs connecting between positive charges of chitosan chains

Despite the fact that the processes of obtaining chitosan NPs by the method of ionotropic gelation are quite well known, the influence of various factors on the particle size requires a deeper study. Attempts were made to optimize the processing parameters of chitosan in the process of ionic gelation [22], but there are no unambiguous systematic conclusions in this area of research.

We have carried out studies on the preparation of *Bombyx mori* ChsNPs by ionotropic gelation using an ionic crosslinking agent, sodium tripolyphosphate (TPP) [23].

The concentration of the chitosan solution varied from 5mg/mL to 10 mg/mL, the concentration of the $Na_5P_3O_{10}$ solution was 1 mg • mL^{-1} at a volume ratio of chitosan-NaTPP = 1:1. Optical and AFM studies of ChsNPs samples were carried out. It was revealed that chitosan nanoparticles with sizes of 50 nm ~ 200 nm with an ordered structure of high intensity were obtained. Figure 5 shows the AFM and topography image of chitosan NPs. The resulting ChsNPs had an immunomodulatory effect on living organisms, increased the number of antibody-forming cells in the spleen, the total number of cells in the central and peripheral organs: thymus, bone marrow, lymph nodes [24], i.e. ChsNPs has a fairly pronounced immunostimulating activity. Our studies are consistent with the literature data of the authors in the work [25] in which the chitosan biopolymer stimulates cellular metabolism and, first of all, activates the functions of immune system cells.

In chemical crosslinking, crosslinkers react with polysaccharides to form either intermolecular or intramolecular covalent bonds. The covalently crosslinked polysaccharide nanoparticles allow the network structure to be permanent as irreversible chemical bonds are formed.

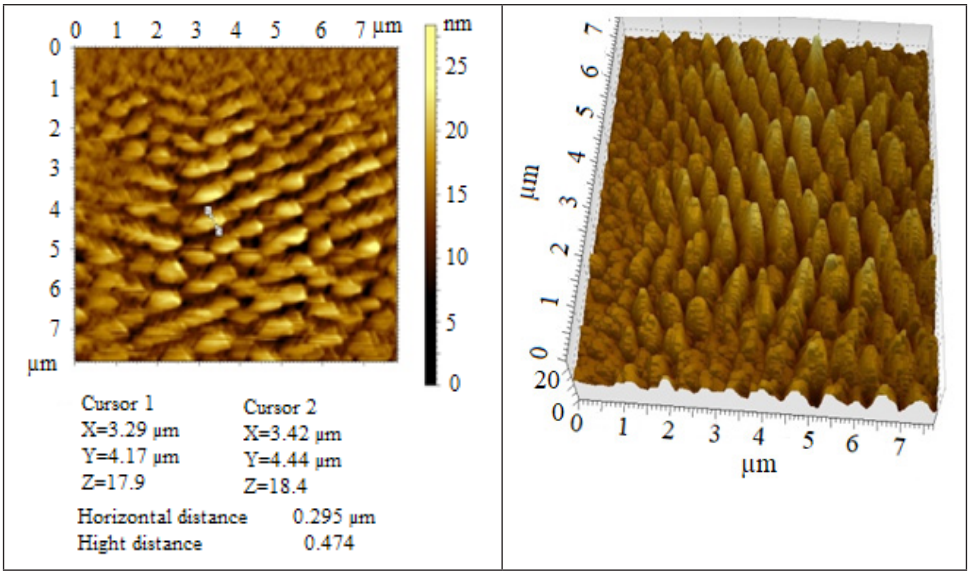

Figure 5. AFM and topography image ChsNPs, concentration of Chs solution - 0.5 mg/mL. The ratio of chitosan:TPP = 3:1, the concentration of $Na_5P_3O_{10}$ is 1 mg/mL. ChsNPs size =295 nm

Despite a sharp change in pH, the rigid network allows the absorption of water and biologically active substances without dissolving the nanoparticles. Crosslinker concentration and crosslinking time affect the degree of chemical crosslinking [20]. Chemical cross-linking is carried out using glutaraldehyde, formaldehyde, genipin, of low-toxic di- and tricarboxylic acids (succinic acid, malic acid, tartaric acid and citric acid), vanillin, epichlorohydrin, etc. [26]. Modification of chitosan can be carried out by crosslinking the molecules of this polysaccharide with biologically active compounds, in particular, glutaraldehyde. The method of cross-linking chitosan by means of glutaraldehyde (GA) is accompanied by the formation of a network supramolecular structure, which, depending on the conformational state and chain stacking, is characterized by different porosity. Of great interest is the ordered stacking of chains during crosslinking, since in this case it is possible to form the same type and evenly spaced pores in the crosslinked polymer and obtain a network material with pronounced anisotropic swelling and desorption properties.

We carried out a study in this direction for solutions of chitosan *Bombyx mori* (M = 110 kDa) in 2% CH_3COOH of various chitosan concentrations (C = 0.15%; 0.25%; 0.50%; 0.75%; 1.0%) by cross-linking with glutaric aldehyde at 25 °C, the modulus of the solution of chitosan and the cross-linking agent was: 5:1. Cross-linking of *Bombyx mori* chitosan with glutaraldehyde occurs at a concentration above 0.75 g/dL.

We have conducted studies on the reparative regeneration of skin cells in thermal injury and the possibility of correcting the identified disorders when using *Bombyx mori* chitosan-based gels cross-linked with glutaraldehyde (GA) and filled with biologically active elements (BAE). Furacilin (FC) was used as BAE, an aqueous solution of which was prepared for experiments by dissolving furacillin powder. The results of freeze drying of the swollen sample showed that cross-linked chitosan contains about 0.5% furacillin in its composition. The morphological (histological) pattern of skin cell regeneration in thermal injury was assessed. During the treatment with gels for burn injury, primary anatomical and functional changes, reactive-inflammatory phenomena and regenerative processes were observed in the affected area. Chitosan gels, especially in combination with furatsilin, significantly increased the regeneration coefficient, which, apparently, determined the earlier reduction of the burn surface (Figure 6).

The obtained data indicate that chitosan has a pronounced ability to accelerate wound healing: chitosan is capable of compacting with cell DNA, which leads to the activation of reparative processes in the nuclear apparatus of the cell and to the regeneration of unburned cells [27]. The presence of furacilin has a bactericidal effect, contributing to faster wound cleansing and earlier skin regeneration, significantly accelerate the healing rate of affected areas, increase the regeneration coefficient, contributing to an earlier reduction of the burn surface.

When tripolyphosphate (TPP) is used as an ionic crosslinking agent, two aqueous phases containing chitosan and another one consisting of polyanionic TPP are mixed to form a complex coacervate [28].

The electrostatic interaction between the cationic amino groups of chitosan and the negatively charged anions of the crosslinker promotes the formation of nanoparticles.

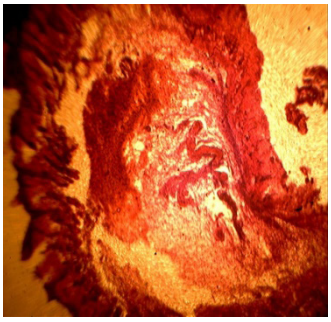	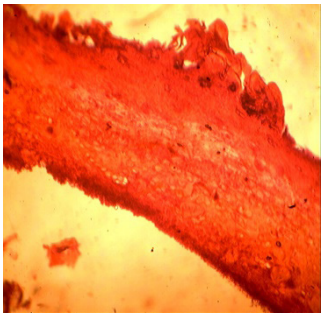	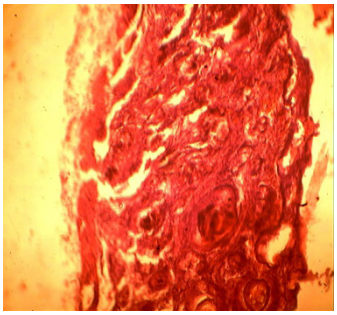
a	b	c
Histopreparation of skin samples of the first group with thermal burn after 3 days. Visible: necrosis and inflammation of the layers of the skin. Increase X 200	*after 7 days. Visible, multilayered flat epithelium, in which layers of the epidermis are determined. The newly formed granulation tissue, blood vessels*	*after 10 days. A newly formed granulation tissue, blood vessels are revealed, which indicates a good regeneration of the skin.*

Figure 6. Results of morphological studies

Chitosan is dissolved in acetic acid to form a polymer solution. The crosslinker is added to water to form a solution in the presence or absence of stabilizing agents such as Tween 80, polyethylene glycol. The crosslinking agent is added to the chitosan solution to form nanoparticles with stirring at room temperature. The size and surface charge of particles can be modified by changing the ratio of chitosan and stabilizer [29]. The resulting nanoparticles can be successfully used as drug carriers for biomedical applications both *in vitro* and *in vivo*.

Chitosan-TPP/vitamin C nanoparticles were obtained by ionotropic gelation between the positively charged amino groups of chitosan-TPP and vitamin C with constant stirring on a magnetic stirrer at room temperature for 1 hour to stimulate crosslinking [30]. The nanoparticles were isolated using ultracentrifugation at 10,000 rpm for 30 min and freeze-dried nanoparticles were stored for further use. ChsNP can be used as intranasal delivery for migraine therapy. Chitosan nanoparticles containing chitosan sumatrin-succinate are used to treat migraine, to improve the therapeutic effect and reduce the frequency of dosing. For the formation of nanoparticles, the method of ionic gelation was used.

For the treatment of Alzheimer's disease by ionic gelation, the authors of the investigation [31] obtained encapsulated chitosan nanoparticles for delivery to the brain through the nose. To do this, for the formation of nanoparticles, different ratios of thymoquinone were included in the chitosan solution. Other groups have also used the ionic gelation method to prepare vitamin C-containing chitosan nanoparticles *via* the gastrointestinal tract and to induce the non-specific immune system. It has been shown that chitosan nanoparticles are suitable for encapsulating vitamin C in nanoscale and maintaining the immunostimulating properties of vitamin C. Some researchers modified the ionic gelation method to obtain chitosan nanoparticles containing ampicillin trihydrate and evaluated their antimicrobial activity [32].

Staphylococcus aureus microorganisms were used to test the antimicrobial properties of such nanoparticles. They suggested that the concentration of the reagents - polymer and crosslinking agent, as well as the time of sonication are factors limiting the development of optimized nanoparticle compositions. Chitosan nanoparticles were capable of sustained delivery of ampicillin trihydrate.

Another group has also used a modified ionic gelation method to prepare dopamine-containing chitosan nanoparticles for the treatment of Parkinson's disease [33]. The formation of nanoparticles containing dopamine, a neurotransmitter, may help in the treatment of patients with Parkinson's disease.

3.3 Microemulsion Method

Reverse micelles are thermodynamically more stable liquid mixtures of water, oil and surfactant. Macroscopically, they are homogeneous and isotropic and, on a microscopic scale, are structured into water and oil microdomains separated by a film enriched with a surfactant. Surfactants are amphiphilic molecules that spontaneously form spherical or ellipsoidal aggregates (micelles) in the presence of water or an organic solvent. There are conventional micelles that exist in water at a relatively low concentration of organic solvents. Reverse micelles are

formed in a large number of organic solvents such as hydrocarbons (e.g. hexane, octane, isooctane or benzene), long chain alcohols, chloroform, diethyl ether, etc. In reverse micelles, the reaction takes place in the water core of reverse micellar droplets [34]. Here, aqueous solutions of the monomer, crosslinking agent, and other hydrophilic compounds remain in the water core (host- nanoreactor) of reverse micelles (Figure 7).

The polymerization reaction leading to the formation of nanoparticles occurs in these aqueous media through the primary growth process. Reverse micellar droplets are nanometer sized, so any polymerization reaction taking place in these droplets will result in nanometer sized polymers.

Reverse micellar drops consist of a swollen water core stabilized by a layer of surfactant molecules and dispersed in oil. The process of nucleation in such a system is continuous and can proceed during the entire polymerization reaction. The number of polymer particles formed steadily increases with time, but their size remains constant.

The authors obtained chitosan nanoparticles using the microemulsion method by involving chitosan in the water core of the reverse micellar system, followed by crosslinking with glutaraldehyde [35]. Chitosan nanoparticles were formed using a surfactant, such as AOT - sodium bis (2-ethylhexyl) sulfosuccinate. Initially, the surfactant was dissolved in n-hexane, and then chitosan and glutaraldehyde were added to the surfactant/n-hexane mixture with continuous stirring at room temperature. The free amino groups of chitosan were crosslinked with glutaraldehyde, the organic solvent was removed by evaporation at low pressure, followed by the accumulation of crosslinked chitosan nanoparticles. Excess surfactant was removed by precipitation with $CaCl_2$ and then centrifuged. The size of lyophilized nanoparticles was less than 100 nm. In addition, the size can be controlled by changing the concentration of glutaraldehyde.

The authors of the article [36] prepared chitosan-alginate nanoparticles with a core and a shell using a reversible water-in-oil microemulsion. The study concludes that these biocompatible and biodegradable nanoparticles can be used to encapsulate plasmid DNA for gene delivery via the cellular pathway of endocytosis.

In one of the studies, chitosan nanoparticles were obtained by the authors by cross-linking reverse micellar droplets with glutaraldehyde in the aqueous core [37]. An optically transparent solution was obtained by resuspension of chitosan nanoparticles in an aqueous buffer. The pH-dependent recovery of adsorbed oligonucleotides from nanoparticles *in vitro* showed that the recovery of oligonucleotides at alkaline pH is higher compared to neutral and acidic media.

3.4. Covalent Linking Method

Chitosan has the ability to form covalent bonds with various functional crosslinkers. This method for producing nanoparticles involves the formation of covalent bonds between chitosan chains with agents such as polyethylene glycol (PEG), dicarboxylic acid, glutaraldehyde, or monofunctional agents such as epichlorohydrin. Chitosan has amino groups that are protonated in an acidic aqueous solution, making it soluble in it. But it is insoluble in other solutions, which limits its use. Thus, to make it soluble in

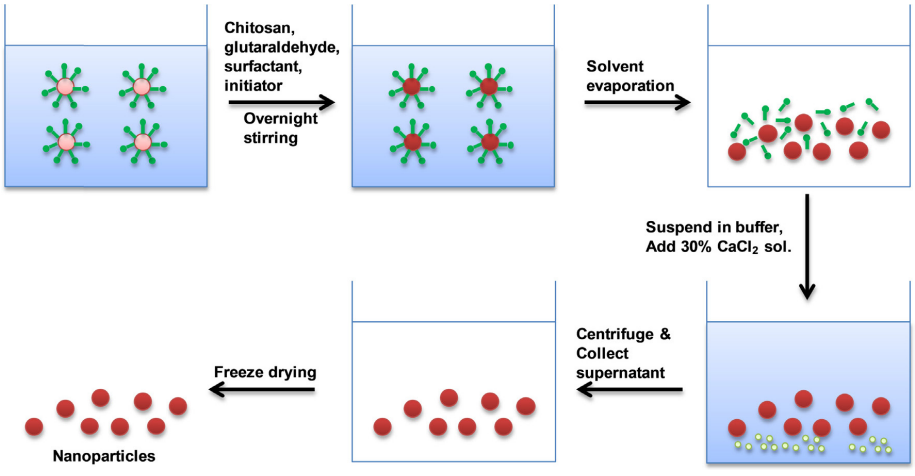

Figure 7. Microemulsion method: in reverse micelles, the reaction takes place in the water core of reverse micellar droplets.

water or other organic solvents, chitosan can be modified by the addition of PEG or other cross-linking agent.

Such attempts can be made by grafting chitosan through chemical modifications with other polymers such as PEG with different M_W [38]. PEGylation of chitosan through hydroxyl groups was first performed by Gorokhovtseva and Makushka [39]. To obtain PEGylated chitosan nanoparticles, chitosan molecules are chemically selectively modified with PEG at the C-6 position of the glucosamine units. Using phthalic anhydride, the amino groups at the C-6 position are protected. Sodium hydride (NaH) is used for catalytic esterification between chitosan and PEG. These PEGylated chitosan nanoparticles are used for gene/drug delivery.

We have obtained nanopolymers based on chitosan *Bombyx mori* and polyethylene glycol (PEG), which were synthesized by graft copolymerization to obtain water-soluble hybrid systems that combine the properties of natural and synthetic polymers [40].

The synthesis of PEG-O-ChsBm graft copolymers was carried out by a sequence of 4 stages: (1) the synthesis of polyethylene glycol monomethyl ether iodide based on the activation of PEG monomethyl ether using triphenyl phosphate to prevent hydrolysis of the product, (2) the protection of chitosan amino groups with a threefold excess of phthalic anhydride in the atmosphere N_2, (3) reaction of N-phthaloyl chitosan and polyethylene glycol monomethyl ether iodide and (4) removal of N-phthaloyl groups by hydrazine monohydrate (Figure 8).

PEG-O-ChsBm amphiphilic graft copolymers spontaneously self-assemble in an aqueous medium and generate 3D supramolecular assemblies by forming hydrogen bonds between unmodified glucosamine units of chitosan.

Various interactions contribute to the self-organization process, namely, electrostatic interactions of the amino groups of chitosan, hydrophobic interactions of $-CH_2-CH_2$ and acetyl groups, and H-bonds involving the -OH group of chitosan [41].

The solubilization effect of PEG chains on chitosan is based on a decrease in the number of hydrogen bonds between chitosan units caused by the presence of PEG chains [42].

Supramolecular 3D ensembles were characterized by various modern methods: IR and ^{1}H-NMR spectroscopy, a combination of TEM, SEM and cryo-TEM (Figure 9).

The toxicity of the nanoparticles was assessed by HeLa and THP-1 cell lines (Figure 10). The results of the experiments revealed the absence of toxicity, which may

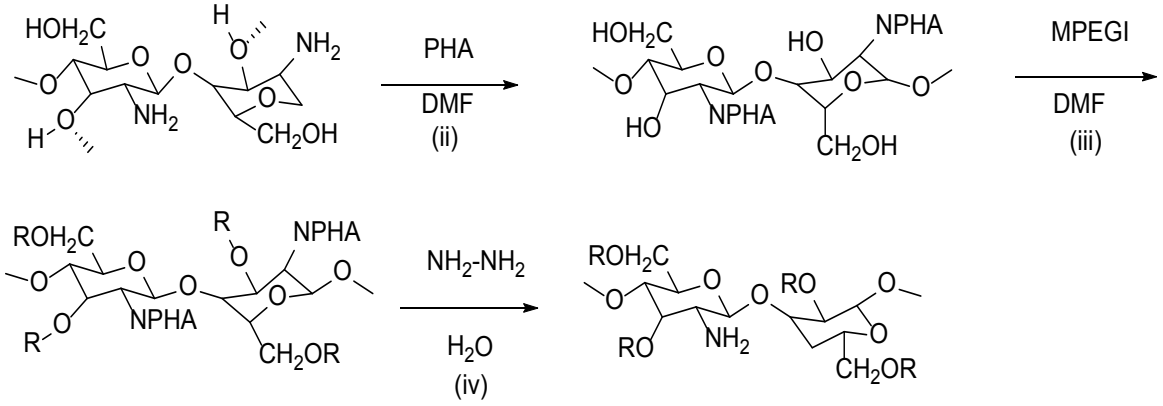

Figure 8. O-PEGylation of Bombyx Mori chitosan, where R: $CH_2CH_2(OCH_2CH_2)_mOCH_3$ and PHA: phthalic anhydride

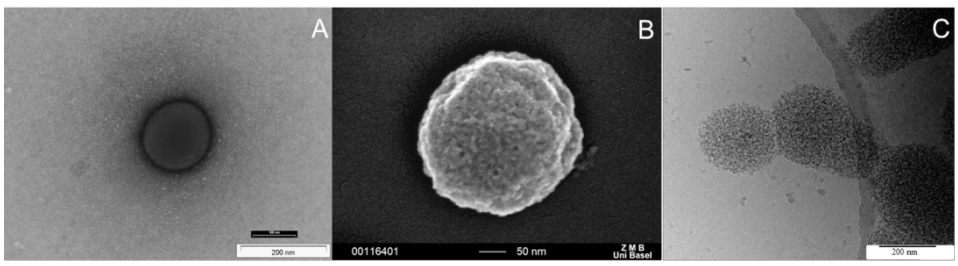

Figure 9. Nanoparticles produced by self-assembly of PEG-O-X3Bm 1.12 tested by TEM: (A) Scale: 200 nm, (B) SEM. Scale: 50 nm , and (C) cryo-TEM. Scale: 200 nm.

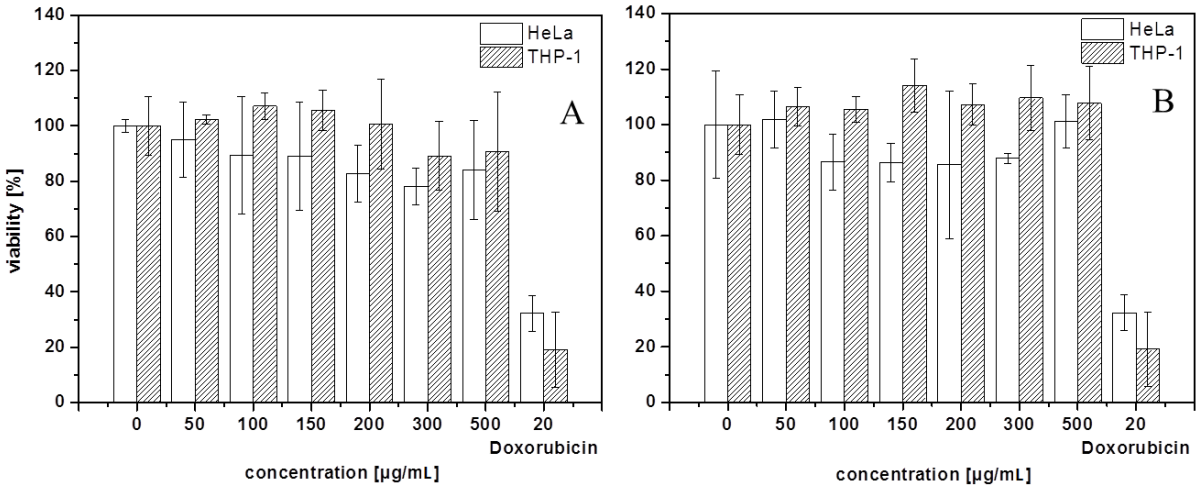

Figure 10. HeLa and THP-1 cell viability after 24 h incubation (A) PEG-O-ChsBm1.12 and (B) PEG-O-ChsBm0.70 nanoparticles.

contribute to the potential medical application of PEG-O-ChsBm nanoparticles for protein attachment.

Chitosan and polyethylene glycol based nanosystems are ideal candidates for on-demand drug delivery through direct selection of their properties that will support a wide range of biomedical applications.

3.5 Method of Incorporation and Incubation

This method is usually used to obtain chitosan nanoparticles for the delivery of protein molecules. In the incorporation method, the protein is first pre-mixed with a chitosan solution, and the pH is adjusted to 5.5 at a temperature of 20 °C [43]. Further mixing of the protein-chitosan solution with TPP leads to the spontaneous formation of chitosan-protein nanoparticles, followed by gentle stirring for 60 mins. During the process of association, protein molecules are introduced into the chitosan-protein nano-matrix, and some protein molecules are absorbed on the surface of the particle. On the contrary, in the incubation method, chitosan nanoparticles are first formed through coacervation of TPP followed by mixing with solutions containing protein at specified concentrations. These solutions are gently stirred for 60 min to ensure that the protein is adsorbed onto the nanoparticles to achieve isothermal equilibrium. In this method, the protein is involved exclusively due to adsorption on the surface of nanoparticles [44].

No less interesting are the data on AFM studies carried out during the preparation of the protein-chitosan complex *Bombyx mori* [45].

When analyzing the supernatant that formed after the precipitation of the complex and its separation, by AFM method nanoparticles with sizes of 100 nm~600 nm were detected. The driving forces in the formation of protein and chitosan complexes during the separation phase are electrostatics and the force of attraction between the aggregates, which become stronger when the charge density increases.

In thermodynamically compatible systems, proteins and polysaccharides have opposite charges, resulting in electrostatic discharge. When protein-polysaccharide complexes are induced electrostatically, it is assumed that stabilization must be achieved through secondary hydrogen bonds or hydrophobic interactions [46]. The results obtained by determining the particle size of the complexes in an aqueous medium revealed the formation of associates (macromolecular nanostructures) with sizes from 150 nm to 600 nm (Figure 11a). The surface cut profile (Figure 11b) showed a value of 47.9 nm. Polymer complexes in a solvent exist in the form of a globular coil, are highly mobile, and are capable of assuming various conformations. These data are consistent with the work of the authors [47], which showed that, due to the small size of the complexes, they have a high specific surface area and exhibit high physicochemical activity and sorption capacity.

3.6 Solvent Evaporation Method

The method includes the formation of an emulsion of chitosan followed by evaporation of the solvent. At the initial stage, the chitosan solution is added to the aqueous phase to form an emulsion. The evaporation of the polymer solvent then leads to the formation of nanospheres due to precipitation. Chitosan is added to ethanol, and then the pDNATris buffer is added to this solution with

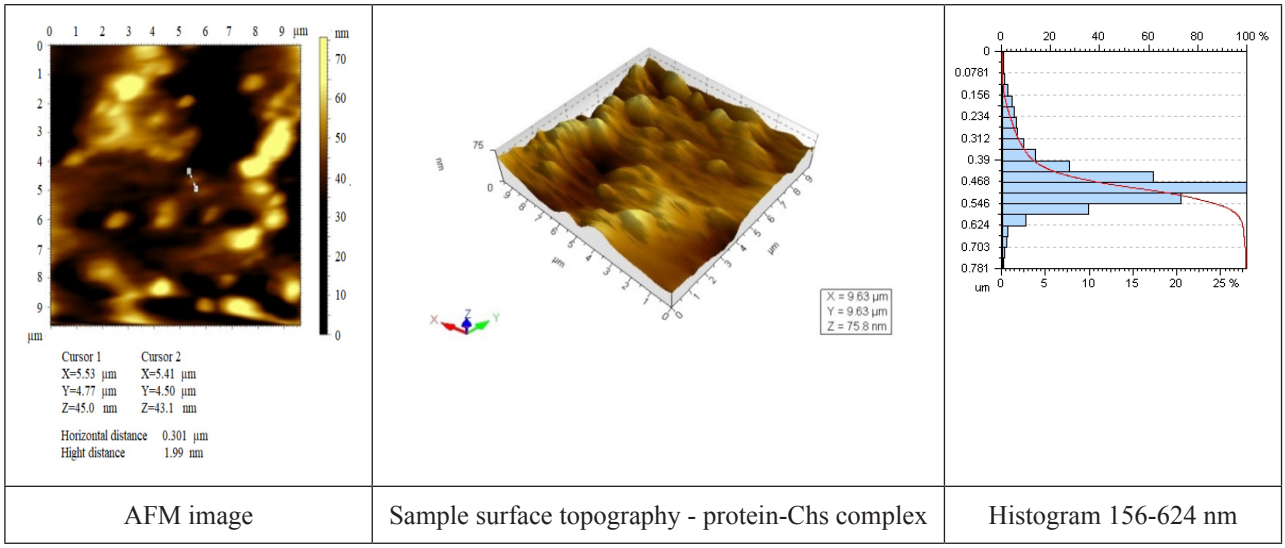

a

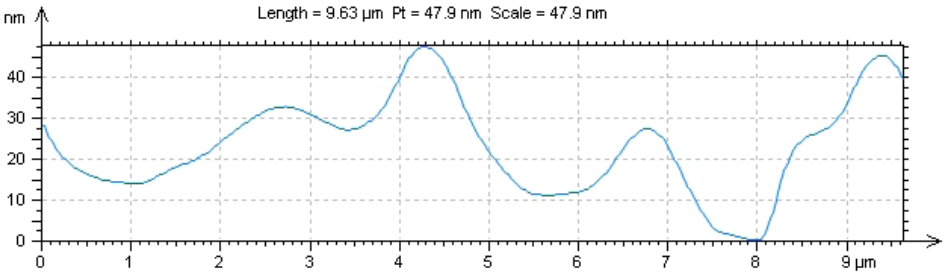

b

Figure 11. AFM-images - - protein-Chs complex -a, b- profile

rapid pouring of ethanol while stirring on a magnetic stirrer. By applying reduced pressure, the solvent is removed from the obtained nanoparticles. The authors of investigation [48] prepared cyclosporine-A loaded with modified lipid-based nanoparticles with PEGylated chitosan using the emulsification/solvent evaporation method, where the average nanoparticle size was 89.4 nm. It was found that the efficiency of encapsulation of cyclosporine - A on nanoparticles modified with chitosan is 69.22%. In another published study, the authors of the work [49] used the modified solvent evaporation method to obtain nanoparticles in two size ranges of 126 nm~139 nm and 151 nm~181 nm. Lectin/chitosan nanoparticles were loaded with hydrochlorothiazide (HCT) and then in complex with β-cyclodextrin (HCT-β-CD). The maximum entrainment efficiency of 81.8 ± 1.7% and 91.1 ± 1.5% was obtained for nanoparticles loaded with HCT and HCT-β-CD, respectively.

3.7 Co-precipitation Method

This method involves the co-precipitation of a chitosan solution obtained in a low pH acetic acid solution by adding an ammonium hydroxide solution to a high pH of 8.5-9.0, resulting in the formation of highly dispersed chitosan nanoparticles. In a published investigation, chitosan nanoparticles grafted with lactic acid were obtained by coprecipitation with the addition of Chs with lactic acid to ammonium hydroxide to form coacervate droplets. The resulting nanoparticles were highly monodisperse with a size of ~10 nm [50]. In another study by research [51] obtained magnetic nanoparticles coated with chitosan by co-precipitation using various concentrations of chitosan. Chitosan and 6-mercaptopurine nanoparticles were obtained by this method and used as a drug delivery system [52].

To obtain nanoparticles, we used *Bombyx mori* Chs isolated from silkworm pupae, which are waste products of silk production. Synthesis of nanochitosan from *Bombyx mori* Chs was carried out by fractional coprecipitation in the presence of TWEEN-80 surface modifier. It was shown that TWEEN-80 prevents the agglomeration of nanoparticles, which makes it possible to obtain freeze-dried nanoparticles in the form of a dry powder. The particle

size of nanochitosan is 90 nm~200 nm. The sensitivity test of strains of microorganisms related to gram-positive was carried out: *Aureus, St.epidermidis, St.saprofiticus, Str.pyogens, Enteroc. faecalis*; microorganisms related to gram-negative bacteria - *Esch. Coli LP, Esch. Coli LN, Prot. vulgaris, Klebsiella, Ps. aerogenosa;* and microorganisms related to fungi - *Candida albicans, Actinomyces, Bas. Subtilis* to the action of Chs nanoparticles. It is shown that, depending on the concentration, chitosan has an antibacterial effect on almost all groups of microorganisms: *St.saprofiticus, Str.pyogens, Ent.faecalis, Esch. Coli LP, Esch. Coli LN, Prot. vulgaris, Klebsiella, Actinomyces*. In addition, nanochitosan has an immunostimulating effect on living organisms, which makes it possible to recommend preparations based on nanochitosan for raising immunity [53].

3.8 Complex Coacervation Method

The complex coacervation method was used to obtain chitosan nanoparticles by forming coacervates between cationic chitosan and anionic polyanions, polymers, or biomacromolecules. The authors of the article [54] obtained nanoparticles of chitosan-poly(acrylic acid), where it was observed that the size depends on the ratio between the two polyelectrolytes.

pH-sensitive chitosan/poly(acrylic acid) nanospheres with a diameter of 70 nm to 500 nm were prepared by emulsion polymerization of acrylic acid in the presence of chitosan.

Figure 12 shows the interaction between chitosan and polyacrylic acid, which leads to the formation of nanospheres. As shown in Figure 12, acrylic acid molecules are electrostatically bonded to chitosan, forming a micelle framework.

During polymerization, polyacrylic acid (PAA) interacts with chitosan at the interface of micelles. The contraction of the spheres through electrostatic interaction between chitosan and PAA, as well as the expansion of spheres due to the electrostatic repulsion of chitosan molecules, phase separation between the polymer and the solvent lead to the formation of polymeric nanostructures - PNS.

Chitosan/alginate nanoparticles have been obtained for the delivery of bioactive molecules such as proteins and nucleic acids [55]. The authors of the investigation [56] obtained chitosan nanoparticles using chitosans of different molecular weights and DDA, quaternized chitosans, and a trimethylated chitosan oligomer to encapsulate plasmid DNA encoding green fluorescent protein (GFP) using complex coacervation.

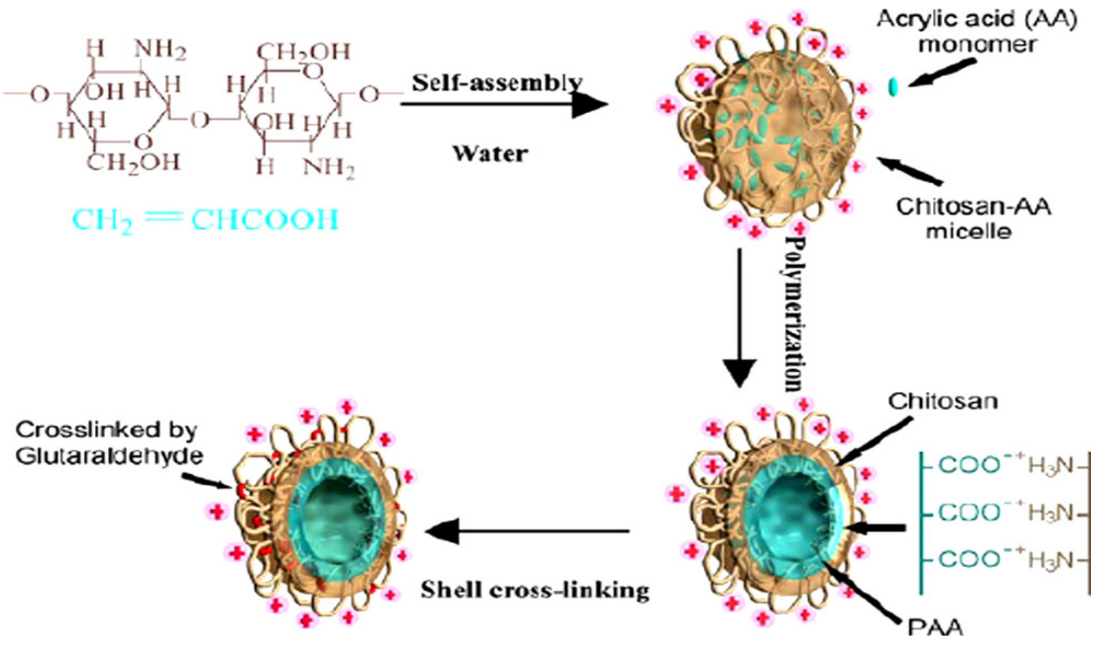

Figure 12. Scheme of the formation of chitosan/poly(acrylic acid) nanospheres

4. Conclusions

Numerous publications on the study of nanomaterials based on chitosan and its derivatives reflect the importance of this polymer. Major fundamental and technical advances have been used to increase the feasibility and improve the properties and reliability of chitosan-based nanomaterials for various applications. Chitosan and chitosan-based nanomaterials are amazing materials that have a wide range of promising applications. Chitosan can be modified with various functional groups to control hydrophobic, cationic and anionic properties. That is why chitosan is a relatively unique biopolymer. These specific properties of chitosan are the result of the presence of primary amino groups in its chain. This structure gives these polysaccharides not only very valuable physical and chemical properties, but also special interactions with cells, proteins and living organisms. Modified chitosan has an excellent ability to immobilize biomolecules, which demonstrates great potential for creating the basis of drugs.

Depending on the requirements, chitosan is functionalized to achieve targeted delivery. Thus, it is clear that chitosan nanoparticles have the potential for efficient drug/gene delivery to target organs. Therefore, the unique specificity of the properties of chitosan and nanomaterials derived from it, with the properties inherent in this natural polymer, can serve as a promising future, demonstrating emerging products on the market, especially in the field of medicine. It is reasonable to expect significant advances in the application of chitosan and nanomaterials based on it, with extensive innovative possibilities that will fundamentally change the field of nanotechnology in the near future.

Conflict of Interest

There is no conflict of interest.

References

[1] Birrenbach, G., Speiser, P.P., 1976. Polymerized micelles and their use as adjuvants in immunology. Journal of Pharmaceutical Sciences. 65, 1763-1766.

[2] Peer, D., Karp, J.M., Hong, S., et al., 2007. Nanocarriers as an emerging platform for cancer therapy. Nature nanotechnology. 2, 751-760.

[3] Adeli, M., Mirab, N., Zabihi, F., 2009. Nanocapsules based on carbon nanotubes-graft-polyglycerol hybrid materials. Nanotechnology. 20, 485603.

[4] Yi, H., Wu, L.Q., Bentley, W.E., et al., 2005. Biofabrication with chitosan. Biomacromolecules. 6, 2881-2894.

[5] Aiba, S., 1992. Studies on chitosan: 4. Lysozymic hydrolysis of partially N-acetylated chitosans. International Journal of Biological Macromolecules. 14, 225-228.

[6] Zhang, H., Neau, S.H., 2002. In vitro degradation of chitosan by bacterial enzymes from rat cecal and colonic contents. Biomaterials. 23, 2761-2766.

[7] Escott, G.M., Adams, D.J., 1995. Chitinase activity in human serum and leukocytes. Infection and Immunity. 63, 4770-4773.

[8] Huang, M., Fong, C.W., Khor, E., et al., 2005. Transfection efficiency of chitosan vectors: effect of polymer molecular weight and degree of deacetylation. Journal of Controlled Release. 106, 391-406.

[9] Ozgel, G., Akbuga, J., 2006. In vitro characterization and transfection of IL-2 gene complexes. International Journal of Pharmacy. 315, 44-51.

[10] MacLaughlin, F.C., Mumper, R.J., Wang, J., et al., 1998. Chitosan and depolymerized chitosan oligomers as condensing carriers for in vivo plasmid delivery. Journal of Controlled Release. 56, 259-272.

[11] Richardson, S.C., Kolbe, H.V., Duncan, R., 1999. Potential of low molecular mass chitosan as a DNA delivery system: biocompatibility, body distribution and ability to complex and protect DNA. International Journal of Pharmacy. 178, 231-243.

[12] Borchard, G., 2001. Chitosans for gene delivery. Advanced Drug Delivery Reviews. 52, 145-150.

[13] Guliyeva, U., Oner, F., Ozsoy, S., et al., 2006. Chitosan microparticles containing plasmid DNA as potential oral gene delivery system. European Journal of Pharmaceutics and Biopharmaceutics. 62, 17-25.

[14] Mansouri, S., Lavigne, P., Corsi, K., et al., 2004. Chitosan-DNA nanoparticles as non-viral vectors in gene therapy: strategies to improve transfection efficacy. European Journal of Pharmaceutics and Biopharmaceutics. 57, 1-8.

[15] van der Lubben, I.M., Verhoef, J.C., Borchard, G., et al., 2001. Chitosan and its derivatives in mucosal drug and vaccine delivery. European Journal of Pharmaceutical Sciences. 14, 201-207.

[16] Sharma, S., Mukkur, T.K., Benson, H.A., et al., 2012. Enhanced immune response against pertussis toxoid by IgA-loaded chitosan-dextran sulfate nanoparticles. Journal of Pharmaceutical Sciences. 101, 233-244.

[17] Nam, J.P., Choi, C., Jang, M.K., et al., 2010. Insulin-incorporated chitosan nanoparticles based on polyelectrolyte complex formation. Macromolecular Research. 18, 630-635.

[18] Liu, Z., Jiao, Y., Liu, F., et al., 2007. Heparin/chitosan nanoparticle carriers prepared by polyelectro-

lyte complexation. Journal of Biomedical Materials Research Part A. 83A, 806-812.

[19] Janes, K.A., Fresneau, M.P., Marazuela, A., et al., 2001. Chitosan nanoparticles as delivery systems for doxorubicin. Journal of Controlled Release. 73, 255-267.

[20] Crini, G., 2005. Recent developments in polysaccharide-based materials used as absorbents in waste water treatment. Progress in Polymer Science. 30, 38-70.

[21] Peniche, H., Peniche, C., 2011. Chitosan nanoparticles: a contribution to nanomedicine. Polymer International. 60, 883-889.

[22] Huang, Y., Lapitsky, Y., 2011. Monovalent salt enhances colloidal stability during the formation of chitosan/tripolyphosphate microgels. Langmuir. 27, 10392-10399.

[23] Milusheva, R.Yu., Rashidova, S.Sh., 2022. Obtaining chitosan nanoparticles from *Bombyx mori*. Russian Chemical Bulletin, 71(2), 232-239.

[24] Rashidova, S.Sh., Milusheva, R.Yu., 2010. Nanostructured polysaccharides on the chitosan *Bombyx mori* base and possibility their using in medicine. 6th Nanofun-poly Conference. pp. 92. Madrid.

[25] Ivanushko, L.A., 2007. Comparative study of the immunomodulatory properties of chitosan and its derivatives. Medical Immunology. 9(4-5), 397-404.

[26] Carmen, R., Roland, L., 1997. Mechanical, water uptake and permeability properties of cross-linked chitosan glumate and alginate films. Journal of Controlled Release. 44, 215-225.

[27] Kadirova, D.A., Inoyatova, F.Kh., Baikulov, A.K., et al., 2022. Study of the binding of chitosan to specific DNA regions in the treatment of thermal burns. Bulletin of NGU. Series: Biology, clinical medicine. 10(5). 31-36. http://elibrary.ru (Access on 20 May 2022).

[28] Pan, Y., Li, Y.J., Zhao, H.Y., et al., 2002. Bioadhesive polysaccharide in protein delivery system: chitosan nanoparticles improve the intestinal absorption of insulin in vivo. International Journal of Pharmacy. 249, 139-147.

[29] Lopez-Leon, T., Carvalho, E.L., Seijo, B., et al., 2005. Physicochemical characterization of chitosan nanoparticles: electrokinetic and stability behavior. Journal of Colloid and Interface Science. 283, 344-351.

[30] Alishahi, A., Mirvaghefi, A., Tehrani, M.R., et al., 2011. Chitosan nanoparticle to carry vitamin C through the gastrointestinal tract and induce the non-specific immunity system of rainbow trout (Oncorhynchus mykiss). Carbohydrate Polymers. 86, 142-146.

[31] Alam, S., Khan, Z.I., Mustafa, G., et al., 2012. Development and evaluation of thymoquinone-encapsulated chitosan nanoparticles for nose-to-brain targeting: a pharmacoscintigraphic study. International Journal of Nanomedicine. 7, 5705-5718.

[32] Saha, P., Goyal, A.K., Rath, G., 2010. Formulation and evaluation of chitosan-based ampicillin trihydrate nanoparticles. Tropical Journal of Pharmaceutical Research. 9, 483-488.

[33] De Giglio, E., Trapani, A., Cafagna, D., et al., 2011. Dopamine-loaded chitosan nanoparticles: formulation and analytical characterization. Analytical and Bioanalytical Chemistry. 400, 1997-2002.

[34] Bellocq, A.M., Biais, J., Bothorel, P., et al., 1984. Microemulsions. Advances in Colloid and Interface Science. 20, 167-272.

[35] Banerjee, T., Mitra, S., Kumar Singh, A., et al., 2002. Preparation, characterization and biodistribution of ultrafine chitosan nanoparticles. International Journal of Pharmacy. 243, 93-105.

[36] You, J.O., Liu, Y.C., Peng, C.A., 2006. Efficient gene transfection using chitosan-alginate core-shell nanoparticles. International Journal of Nanomedicine. 1, 173-180.

[37] Manchanda, R., Nimesh, S., 2010. Controlled size chitosan nanoparticles as an efficient, biocompatible oligonucleotides delivery system. Journal of Applied Polymer Science. 118, 2071-2077.

[38] Sugimoto, M., Morimoto, M., Sashiwa, H., et al., 1998. Preparation and characterization of water-soluble chitin and chitosan derivatives. Carbohydrate Polymers. 36, 49-59.

[39] Gorochovceva, N., Makuška, R., 2004. Synthesis and study of water-soluble chitosan-O-poly(ethylene glycol) graft copolymers. European Polymer Journal. 40, 685-691.

[40] Vasquez, D., Milusheva, R., Baumann, P., et al., 2014. The amine content of PEGylated chitosan Bombyx mori nanoparticles acts as a trigger for protein delivery. Langmuir., 30(4), 965-975.

[41] Yang, X.D., Zhang, Q.Q., Wang, Y.S., et al., 2008. Self-aggregated nanoparticles from methoxy poly(ethylene glycol)-modified chitosan: Synthesis; characterization; aggregation and methotrexate release in vitro. Colloids and Surfaces B: Biointerfaces, *B. 61*(2), 125-131.

[42] Ouchi, T., Nishizawa, H., Ohya, Y., 1998. Aggregation phenomenon of PEG-grafted chitosan in aqueous solution. Polymer. *39*(21), 5171-5175.

[43] Gan, Q., Wang, T., 2007. Chitosan nanoparticle as protein delivery carrier—Systematic examination of fabrication conditions for efficient loading and release. Colloids and Surfaces B: Biointerfaces. 59, 24-34.

[44] Moghaddam, F.A., Atyabi, F., Dinarvand, R., 2009. Preparation and in vitro evaluation of mucoadhesion and permeation enhancement of thiolated chitosan-pHEMA core-shell nanoparticles. Nanomedicine. 5, 208-215.

[45] Yu, R., Milusheva, O.B., Avazova, S.Sh., 2020. Rashidova Protein from pupae of the silkworm Bombyx mori L. Isolation, properties, application FAN, Tashkent. pp. 216. https://www.livelib.ru/publisher/17911-fan (Access on 20 May 2022)

[46] Schmitt, C., Sanchez, C., Desobry-Banon, S., et al., 1998. Structure and technofunctional properties of protein-polysaccharide complexes: A review. Critical Reviews in Food Science and Nutrition. 38, 689-753.

[47] Jayakumar, R., Menon, D., Manzoor, K., et al., 2010. Biomedical applications of chitin and chitosan based nanomaterials—A short review. Carbohydrate Polymers. 8.

[48] Zhang, L., Zhao, Z.L., Wei, X.H., et al., 2013. Preparation and in vitro and in vivo characterization of cyclosporin A-loaded, PEGylated chitosan-modified, lipid-based nanoparticles. International Journal of Nanomedicine. 8, 601-610.

[49] Chadha, R., Bhandari, S., Kataria, D., et al., 2012. Exploring the potential of lecithin/chitosan nanoparticles in enhancement of antihypertensive efficacy of hydrochlorothiazide. Journal of Microencapsulation. 29, 805-812.

[50] Bhattarai, N., Ramay, H.R., Chou, S.H., et al., 2006. Chitosan and lactic acid-grafted chitosan nanoparticles as carriers for prolonged drug delivery. International Journal of Nanomedicine. 1, 181-187.

[51] Gregorio-Jauregui, K.M., Pineda, M.G., Rivera-Salinas, J.E., et al., 2012. One-step method for preparation of magnetic nanoparticles coated with chitosan. Journal of Nanomaterials. 8.

[52] Dorniani, D., Hussein, M.Z., Kura, A.U., et al., 2013. Preparation and characterization of 6-mercaptopurine-coated magnetite nanoparticles as a drug delivery system. Drug Design, Development and Therapy. 7, 1015-1026.

[53] R.Yu. Milusheva, S.Sh., 2017. Rashidova Bioactive properties of nanochitosan Bombyx mori. Polymer Science, Series C. 59, 29–34.

[54] Hu, Y., Jiang, X., Ding, Y., et al., 2002. Synthesis and characterization of chitosan-poly(acrylic acid) nanoparticles. Biomaterials. 23, 3193-3201.

[55] Gazori, T., Khoshayand, M.R., Azizi, E., et al., 2009. Evaluation of Alginate/Chitosan nanoparticles as antisense delivery vector: formulation, optimization and in vitro characterization. Carbohydrate Polymers. 77, 599-606.

[56] Zheng, F., Shi, X.W., Yang, G.F., et al., 2007. Chitosan nanoparticle as gene therapy vector via gastrointestinal mucosa administration: results of an in vitro and in vivo study. Life Sciences. 80, 388-396.

BILINGUAL PUBLISHING CO.
Pioneer of Global Academics Since 1984

Organic Polymer Material Research
https://ojs.bilpublishing.com/index.php/opmr

ARTICLE

Study of Structural Characteristics of Cellulose Esters with Different Degrees of Substitution

Michael Ioelovich*

Designer Energy, Rehovot, 7670504, Israel

ARTICLE INFO

Article history
Received: 17 June 2022
Revised: 26 July 2022
Accepted: 27 July 2022
Published Online: 29 July 2022

Keywords:
Esters of cellulose
Substitution degree
Structural characteristics
Study
Calculations

ABSTRACT

In this article, structural characteristics of amorphous mono-, di-, and tri-substituted esters of cellulose have been studied. These esters were synthesized under homogenous conditions using anhydrides of various aliphatic acids. The specific gravity of the highly substituted samples was measured by a pycnometric method in the aqueous medium. To calculate the molar, Van der Waals, and free volumes, as well as the packing coefficient of amorphous esters the method of additive contributions of partial volumes of atoms and atom groups in the volumes of polymers was used. Based on the molar volume, also specific gravity of cellulose esters was calculated. The coincidence of calculated and experimental characteristics was shown. In addition, the relationship between glass transition temperature and free volume was found for the esters. The theoretical equations were derived, which provide predicting the structural characteristics of cellulose esters with different degrees of substitution.

1. Introduction

Being a renewable and inexhaustible natural raw material cellulose is widely used for the production of paper and board, powdered and microcrystalline cellulose, cellulose fibers, and films, water-soluble derivatives (carboxymethyl, hydroxyethyl, hydroxypropyl cellulose, etc.), and other products. However, increased hydrophilicity hinders the use of cellulose and its hydrophilic products in the creation of waterproof and vapor-proof materials. Temporary hydrophobization of hydrophilic cellulose materials can be archived by their impregnation with solutions of hydrophobic substances, surface coating, and some other physical or physicochemical methods [1,2]. A more reliable method of cellulose hydrophobization is its chemical modification, especially esterification by replacing hydroxyl groups with hydrophobic substituents [2,3]. For example, it was shown that acetylation of cellulose increases its hydrophobicity and leads to a decrease in the sorption of water vapor [4-7]. As for other cellulose esters, when moving from acetates to higher cellulose esters, the hydrophobicity of cellulose derivatives rises [8].

**Corresponding Author:*
Michael Ioelovich,
Designer Energy, Rehovot, 7670504, Israel;
Email: ioelovichm@gmail.com

DOI: https://doi.org/10.30564/opmr.v4i1.4805

After chemical modification with hydrophobic acyl reagents, the hydrophobic cellulose derivatives can be used in the production of hydrophobic fillers, and reinforcements compatible with hydrophobic polymers, as well as in the compositions of hydrophobic coatings, paints, adhesives, and other hydrophobic materials. Moreover, various cellulose esters, such as acetates, propionates, butyrates, and others are applied in the production of thermoplastics, electronic device housings, spectacle frames, anti-fog goggles, cigarette filters, semi-permeable and separating membranes, optical films, heat, and rot-resistant fabrics, self-cleaning materials, protective coatings, and other materials [1,2,9-11].

Cellulose esterification can be performed under heterogeneous and homogeneous conditions. Heterogeneous esterification of cellulose proceeds in the solid phase according to the laws of topochemical reactions, namely, rapidly in amorphous domains and more slowly inside the cellulose crystallites [12]. In contrast, homogeneous esterification proceeds fairly uniformly in solvent media that swell or/and dissolve cellulose.

After esterification with various acyl reagents, usually, amorphous cellulose derivatives are formed [2]. The problem with studying the supramolecular structure of amorphous esters is that they do not contain crystalline domains, and therefore, the application of such well-known structural methods as X-ray diffraction, electron diffraction, NMR, and some others is difficult. Therefore, little information is currently available on the structure of various amorphous esters of cellulose.

The main purpose of this article was to characterize the structural state of amorphous cellulose esters with different degrees of substitution using such characteristics as molar, Van der Waals, and free volumes, as well as specific gravity.

2. Materials and Methods

The initial cellulose material was pure chemical grade cotton cellulose of Hercules Inc (98% Alfa cellulose, DP= 2700). Using this cellulose, various mono-, di-, and triesters of cellulose were synthesized and studied. Each repeating unit of these esters contained acyl substituents having a different number of carbon atoms (Table 1).

The esterification of the initial cotton cellulose was carried out in the medium of trifluoroacetic acid (TFAA) served as a solvent and also a catalyst [2]. Cotton cellulose was mixed with TFAA while stirring at room temperature for 1 h and then treated with anhydrides of various aliphatic acids at 50 °C for 1 h using a liquid to cellulose ratio of 50. The degree of substitution was adjusted using different molar ratios of anhydrides to cellulose and controlled by a method of chemical analysis [3]. The substitution degree (SD) of monoesters was 0.9-1.1, of diesters 1.8-2.2, and triesters 2.8-3.0. Finally, the cellulose esters were washed and dried in a vacuum chamber at 50 °C to constant weight.

The synthesis scheme of cellulose esters is shown in Figure 1.

Table 1. The studied cellulose esters

Esters of cellulose	Abbreviation	M	Nc
Monoacetate	MAC	204	2
Diacetate	DAC	246	4
Triacetate	TAC	288	6
Monopropionate	MPC	218	3
Dipropionate	DPC	274	6
Tripropionate	TPC	330	9
Monobutyrate	MBC	232	4
Dibutyrate	DBC	302	8
Tributyrate	TBC	372	12
Monovalerate	MVC	246	5
Divalerate	DVC	330	10
Trivalerate	TVC	414	15

M is the molar mass of repeating units (RUs) of various cellulose esters;

Nc is the number of carbon atoms in substituents of RUs

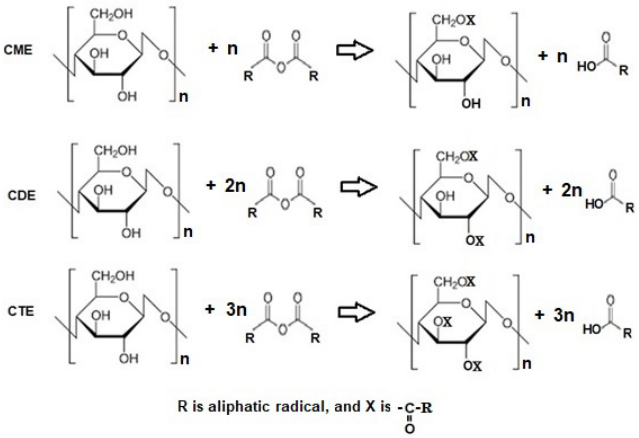

Figure 1. Scheme of cellulose esterification by anhydrides of various aliphatic acids to obtain cellulose mono- (CME), di- (CDE), and tri-(CTE) esters

To evaluate the hydrophobic properties of cellulose esters, the relative hydrophobicity index was used [8]:

$$HI = 100\%\{1 - (A_{es}/A_c)\} \quad (1)$$

where A_{es} (mole H_2O/mole RUs) is the sorption value of water vapor at 25 °C and relative humidity of 80% for various amorphous esters having different SD from 1 to 3, while A_c (mole H_2O/mole RUs) is the sorption value for amorphous cellulose (SD=0) at the same sorption conditions.

The specific gravity of dry triesters was measured by a pycnometric method in the aqueous medium at 23 ºC [13]. For this test, a glass pycnometer, i.e., measurement vessel, with a volume of 25.00 mL was used. The dry sample of cellulose triester having a mass of m (g) was weighed on an analytical balance and then it was placed in the pycnometer, filled with distilled water up to the mark, weighed on the analytical balance, and the weight P was measured. The weight of the empty pycnometer filled with distilled water up to the mark, P_w, was also measured. The specific gravity (G) was calculated as follows:

$$G = g\ m/(P_w + m - P) \quad (2)$$

where g=1 g/cm^3 is the specific gravity of water.

From obtained G values also molar volumes of esters, $V_m = M/G$, were found; where M is the molecular mass of the repeating unit of the ester.

The glass transition temperatures (T_g) of amorphous triesters were determined using thermo-mechanical analysis [14].

To calculate the molar (V_m), Van der Waals (V_w), free (V_f) volumes, as well as packing coefficient of macromolecules ($K_p=V_w/V_m$) of amorphous cellulose esters, the Van Krevelen method of additive contributions of partial volumes of atoms and atom groups in the volumes of polymers was used [15]. The specific gravity of the esters was also calculated, as follows: $G = M/V_m$.

3. Results and Discussion

The results have shown that with an increase in the degree of substitution, the cellulose esters become more hydrophobic (Figure 2).

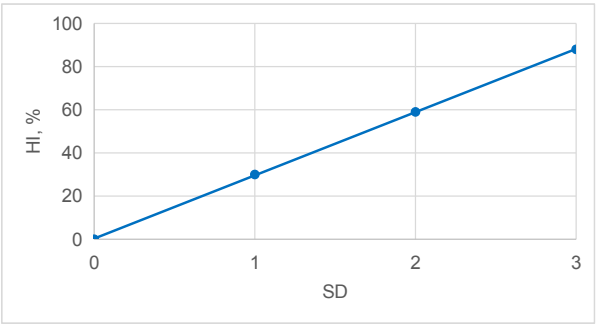

Figure 2. Dependence of relative hydrophobicity on the degree of substitution of esters

The experimental values of the specific gravity for some cellulose esters are shown in Table 2.

As can be seen from Table 2, with an increase in the number of carbon atoms in the substituents, the specific gravity of the studied triesters decreases, and their molar volume increases due to the steric effect of bulk substituents causing enhancement of distances between chains of the esters.

Table 2. Specific gravity (G) and molar volume (V_m) of studied cellulose triesters

Esters of cellulose	M	Nc	G, g/cm^3	V_m, cm^3/mol
TAC	288	6	1.26	228.5
TPC	330	9	1.23	268.0
TBC	372	12	1.16	320.1
TVC	414	15	1.13	365.7

An X-ray study of amorphous cellulose triesters revealed two diffuse scatterings, which are characteristic of a mesomorphic rather than a completely amorphous structure [2]. As a result, model of the mesomorphous structure of cellulose esters was proposed [16]. According to this model, the substituted anhydroglucose units (AGUs) form layers with an approximately constant distance (ca 0.4 nm) between them. However, in the plane of the layers, the distance between substituted AGUs increases directly proportional to the number of carbon atoms, Nc, in the substituents. Based on this model the molar volume and specific gravity of the cellulose triesters were calculated [17], which were actually the same as those presented in Table 2, despite the different investigation methods.

Using the method of additive contributions of partial volumes of atoms and atom groups [15], the molar ($V_{m,sk}$), Van der Waals ($V_{w,sk}$), and free ($V_{f,sk}$) volumes of the skeletons of anhydroglucose units, AGUs, for mono-, di-, and triesters (Figure 3) were calculated (Table 3).

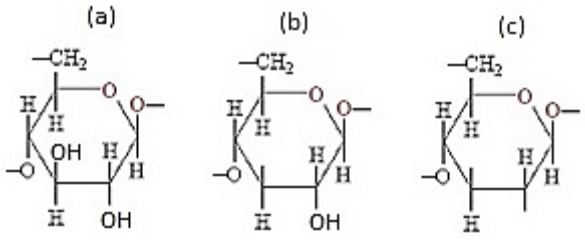

Figure 3. Skeletons of AGUs for mono- (a), di- (b), and tri- (c) esters of cellulose

Table 3. Partial volumes of skeletons of AGUs for cellulose esters

Esters	Skeletons	$V_{m,sk}$, cm^3/mol	$V_{w,sk}$, cm^3/mol	$V_{f,sk}$, cm^3/mol
Monoesters	$C_6H_9O_4$	102.5	73.1	29.4
Diesters	$C_6H_8O_3$	92.8	66.9	25.9
Triesters	$C_6H_7O_2$	83.1	60.7	22.4

The partial volumes of atom groups present in substituents of amorphous esters are shown in Table 4.

Using data presented in Tables 3 and 4, the characteristics of various cellulose esters can be calculated. For example, TBC consists of the skeleton (c), six CH_2-groups,

Table 4. Partial volumes of atom groups of acyl substituents

Group	$V_{m,g}$, cm^3/mol	$V_{w,g}$, cm^3/mol	$V_{f,g}$, cm^3/mol
$-CH_2-$	15.85	10.3	5.55
$-CH_3$	23.9	14.2	9.7
	23.0	16.0	7.0

and three CH_3- and COO-groups. Summing up the contributions of partial volumes of the skeleton and all groups of tributyrate, the molar volume, V_m=318.9 cm^3/mol, Van der Waals volume, V_w = 213.1 cm^3/mol, and free volume, V_f = 105.8 cm^3/mol, for amorphous TBC were calculated. Knowing the Van der Waals and mole volumes, the packing coefficient, K_p = 0.670, and specific gravity, G=1.17 g/cm^3, of TBC were also calculated.

Studies have shown that the structural characteristics of cellulose esters depend both on the degree of substitution and the type of substitute. So, an increase in SD and/or length of the substitute leads to an increase in the molar volume of the esters (Figure 4).

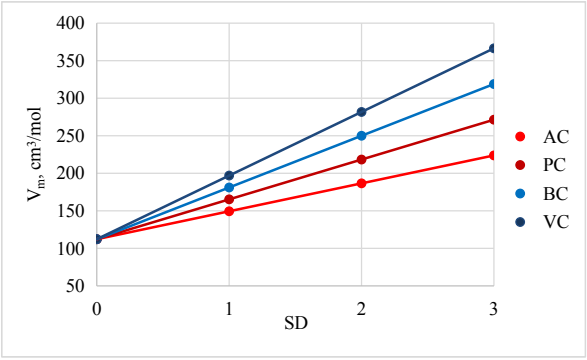

Figure 4. Dependence of molar volume on substitution degree for acetates (AC), propionates (PC), butyrates (BC), and valerates (VC) of cellulose

These dependences can be also expressed by the following theoretical equation:

$$V_m = V_{m,c} + (K_{m,AC} + N\,V_{m,CH2})\,SD \quad (3)$$

where $V_{m,c}$ =112.2 (cm^3/mol) is molar volume of amorphous cellulose; $K_{m,AC}$ = 37.2 is slope factor of dependences V_m = F(SD) for cellulose acetates; and $V_{m,CH2}$ = 15.85 (cm^3/mol) is contribution of partial volume of the CH_2-group in V_m. N is the number of CH_2-groups in one substitute.

Similarly, the theoretical equations for the Van der Waals (V_w) and free ($V_f = V_m - V_w$) volumes were derived.

$$V_w = V_{w,c} + (K_{w,AC} + N\,V_{w,CH2})\,SD \quad (4)$$

where $V_{w,c}$ =79.3 (cm^3/mol) is Van der Waals volume of amorphous cellulose; $K_{w,AC}$ = 24.0 is slope factor of dependences V_w = F(SD) for cellulose acetates; and $V_{w,CH2}$ = 10.3 (cm^3/mol) is contribution of partial volume of the CH_2-group in V_w.

$$V_f = V_{f,c} + (K_{f,AC} + N\,V_{f,CH2})\,SD \quad (5)$$

where $V_{f,c}$ =32.9 (cm^3/mol) is free volume of amorphous cellulose; $K_{f,AC}$ = 13.2 is slope factor of dependences V_f = F(SD) for cellulose acetates; and $V_{f,CH2}$ = 5.55 (cm^3/mol) is contribution of partial volume of the CH_2-group in V_f.

The Equations (3), (4), and (5) provide predicting the structural characteristics of cellulose esters with different degrees of substitution. For example, in acetates the number of CH_2-groups in one substitute, N=0. Then from Equation (3) it follows that for cellulose acetates the dependence V_m = F(SD) will be:

$$V_m\ (cm^3/mol) = 112.2 + 37.2\,SD \quad (6)$$

Another example is cellulose laurates having N=8. In this case, the following dependence can be derived from Equation (3) for these esters:

$$V_m\ (cm^3/mol) = 112.2 + 164\,SD \quad (7)$$

Considering that $K_p = V_w/V_m$ and $G = M/V_m$, the theoretical equations for calculating the packing coefficient of macromolecules (K_p) and specific gravity (G) of various cellulose esters will be the following:

$$K_p = \frac{V_{w,c} + (K_{w,AC} + NV_{w,CH2})SD}{V_{m,c} + (K_{m,AC} + NV_{m,CH2})SD} \quad (8)$$

$$G = M/\{V_{m,c} + (K_{m,AC} + N\,V_{m,CH2})\,SD\} \quad (9)$$

It was found that the packing coefficient has a slight tendency to decrease with increasing SD and/or length of the substitute increases due to the steric effect of bulk substituents. Nevertheless, for studied cellulose esters the average value of K_p = 0.681 ± 0.004, i.e., it is equal to the average K_p value for various solid amorphous polymers [18].

From the Equation (9), it follows that the specific gravity of esters should naturally decrease with an increase in the degree of substitution and/or the length of the substituent (Figure 5).

A comparison of calculations with experimental results indicates a good concordance between them (see e.g., Table 5).

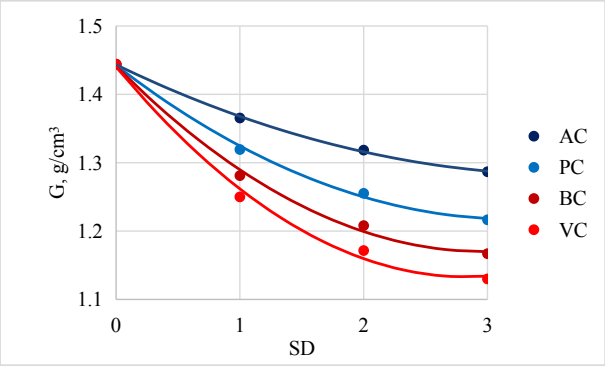

Figure 5. Dependence of specific gravity on substitution degree for acetates (AC), propionates (PC), butyrates (BC), and valerates (VC) of cellulose

Table 5. Calculated and experimental characteristics of cellulose triesters

Esters of cellulose	T_g, °C	V_m, cm³/mol		G, g/cm³	
		Exp	Cal	Exp	Cal
TAC	167	228.5	223.8	1.26	1.28
TPC	130	268.0	271.4	1.23	1.22
TBC	100	320.1	318.9	1.16	1.17
TVC	76	365.7	366.5	1.13	1.13

According to the theory, the glass transition temperature should depend on the free volume of polymers [19]. In this study, an attempt was made to establish such a relationship also for cellulose esters. As a result, the best correlation was found if using the difference between glass temperatures (ΔT_g) and free volumes (ΔV_f) of amorphous cellulose and amorphous triesters (Figure 6).

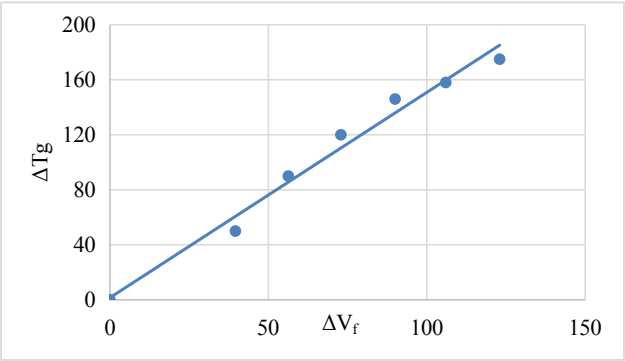

Figure 6. Dependence $\Delta T_g = F(\Delta V_f)$ for amorphous triesters of cellulose

This dependence can be expressed by the equation:

$$\Delta T_g = k\,\Delta V_f \quad (10)$$

where slope factor k=1.5; while $T_{g,c}$ and $V_{f,c}$ for amorphous cellulose are 220 °C [20] and 32.9 cm³/mol, respectively.

This result can be explained by the fact that a larger free volume of cellulose esters provides higher flexibility and mobility of chain segments, which contributes to a decrease in the glass transition temperature.

4. Conclusions

In this article, structural characteristics such as Van der Waals (V_w), molar (V_m), and free (V_f) volumes, as well as packing coefficient of macromolecules (K_p) and specific gravity (G) were used to describe the structural state of amorphous cellulose esters having different degrees of substitution. It was shown that with an increase in the degree of substitution (SD), the cellulose esters become more hydrophobic. Furthermore, the directly proportional dependences of bulk characteristics (V_m, V_w, and V_f) of the esters on SD were found. Conversely, the dependences of specific gravity on SD were nonlinear and inversely proportional. It was also discovered that the average value of packing coefficient K_p =0.681 ± 0.004 for studied cellulose esters is equal to the average K_p value for various solid amorphous polymers.

The theoretical equations were derived, which provide predicting the structural characteristics of cellulose esters with different degrees of substitution. The coincidence of calculated and experimental characteristics was shown. The relationship between glass transition temperature and free volume of cellulose esters was also found.

The introduction of bulk substituents to cellulose causes steric effects resulting in an increase in Van der Waals, molar, and free volumes, as well as a decrease in specific gravity. Moreover, the rise in the free volume of cellulose esters provides higher flexibility and mobility of chain segments, which contributes to a decrease in the glass transition temperature.

Author Contributions

The author conducted research and wrote this article.

Conflict of Interest

The author declares no conflict of interest.

Funding

This research received no funding.

References

[1] Wei, D.W., Wei, H., Gauthier, A.C., et al., 2020. Superhydrophobic modification of cellulose and cotton textiles: Methodologies and applications. Journal Bioresources and Bioproducts. 5, 1-15.

[2] Ioelovich, M., 2021. Adjustment of hydrophobic properties of cellulose materials. Polymers. 13, 1241.

[3] Freire, C.S.R., Silvestre, A.J.D., Neto, C.P., et al., 2005. An efficient method for determination of the degree of substitution of cellulose esters of long chain aliphatic acids. Cellulose. 12, 449-458.

[4] Gocho, H., Shimizu, H., Tanioka, A., et al., 2000. Effect of acetyl content on the sorption isotherm of water by cellulose acetate: comparison with the thermal analysis results. Carbohydrate Polymers. 41, 83-86.

[5] Khoshtinat, S., Carvelli, V., Marano, C., 2021. Moisture absorption measurement and modeling of cellulose acetate. Cellulose. 28, 9039-9050.

[6] Del Gaudio, I., Hunter-Sellars, E., Parkin, I., et al., 2021. Water sorption and diffusion in cellulose acetate: the effect of plasticizers. Carbohydrate Polymers. 267, 118185.

[7] Chalykh, A.E., Bardyshev, I.I., Petrova, T.F., 2021. Free volume and water sorption by cellulose esters. Polymers. 13, 2644.

[8] Ioelovich, M., 2022. Study of water vapor sorption by cellulose esters with different degrees of substitution. World Journal of Advanced Research and Review. 15(1), 214-220.

[9] Edgar, K.J., Buchanan, C.M., Debenham, J.S., et al., 2001. Advances in cellulose ester performance and application. Progress in Polymer Science. 26, 1605-1688.

[10] Filho, G.R., Monteiro, D.S., Da Silva Meireles, K., et al., 2008. Synthesis and characterization of cellulose acetate produced from recycled newspaper. Carbohydrate Polymers. 73, 74-82.

[11] Fischer, S., Thümmler, K., Volkert, B., et al., 2008. Properties and applications of cellulose acetate. Macromolecular Symposia. 262, 89-96.

[12] Sassy, J.F., Chanzy, H., 1995. Ultrastructural aspects of the acetylation of cellulose. Cellulose. 2, 111-127.

[13] ASTM D792-20 Standard, 2020. Test Methods for Density and Specific Gravity (Relative Density) of Plastics by Displacement.

[14] Duncan, J.C., Price, D.M., 2016. Thermomechanical, Dynamic Mechanical and Dielectric Methods. Principles of Thermal Analysis and Calorimetry, 2nd Edition. Simon Gaisford, Vicky Kett and Peter Haines Eds. Royal Soc.: Cambridge. pp. 265.

[15] Van Krevelen, D.W., Nijenhuis, K., 2009. Properties of Polymers: Correlations with Chemical Structure. Elsevier: Amsterdam. pp. 1004.

[16] Ioelovich, M., Laka, M., 2002. Mesomorphous structure of amorphized cellulose esters. Scientific Israel Technological Advantages. 4, 87-89.

[17] Ioelovich, M., 2022. Study of structural characteristics of cellulose esters. Global Journal of Engineering and Technology Advance. 11(3), 24-30.

[18] Askadsky, A.A., 1995. Quantitative analysis of the influence of chemical structure on the physical properties of polymers. Polymer Science Series B. 37, 332-357.

[19] White, R.P., Lipson, J.E., 2016. Polymer free volume and its connection to the glass transition. Macromolecules. 49, 3987-4007.

[20] Ioelovich, M., 2016. Models of supramolecular structure and properties of cellulose. Polymer Science Series A. 58, 925-943.

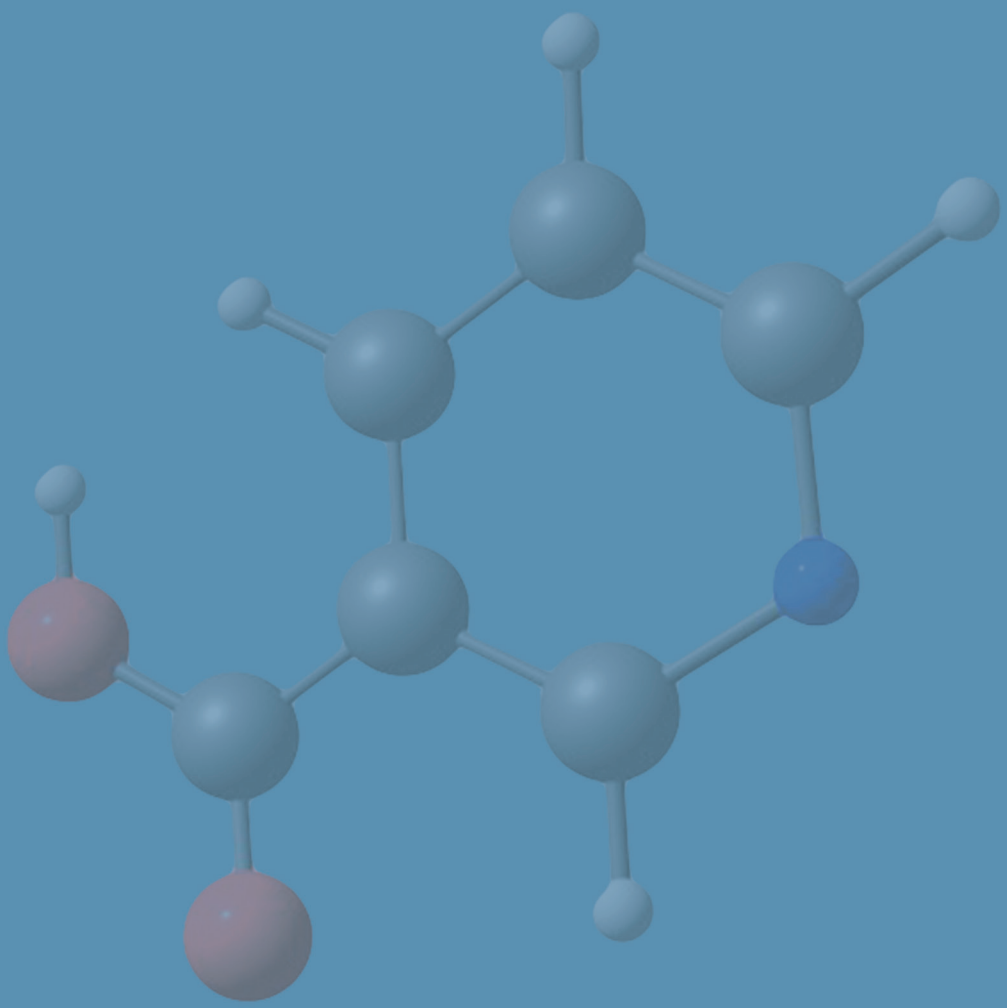

BILINGUAL
PUBLISHING CO.
Pioneer of Global Academics Since 1984

Tel:+65 65881289
E-mail: contact@bilpublishing.com
Website:ojs.bilpublishing.com

2661-3875
01
9 772661 387226